



Sustained Activity of Hippocampal Parvalbumin-Expressing Interneurons Supports Trace Eyeblick Conditioning in Mice

Rongrong Li,^{1*}  Weiwei Zhang,^{1*} Jie Zhang,^{1*} Haibo Zhang,¹ Hui Chen,¹ Zhian Hu,¹ Zhongxiang Yao,¹ Hao Chen,^{2,3} and  Bo Hu^{1,3}

¹Department of Physiology, College of Basic Medical Sciences, Army Medical University, Chongqing 400038, China, ²Experimental Center of Basic Medicine, College of Basic Medical Sciences, Army Medical University, Chongqing 400038, China, and ³Brain and Intelligence Research Key Laboratory of Chongqing Education Commission, Army Medical University, Chongqing 400038, China

Although recent studies have revealed an involvement of hippocampal interneurons in learning the association among time-separated events, its underlying cellular mechanisms remained not fully clarified. Here, we combined multichannel recording and optogenetics to elucidate how the hippocampal parvalbumin-expressing interneurons (PV-INs) support associative learning. To address this issue, we trained the mice (both sexes) to learn hippocampus-dependent trace eyeblink conditioning (tEBC) in which they associated a light flash conditioned stimulus (CS) with a corneal air puff unconditioned stimuli (US) separated by a 250 ms time interval. We found that the hippocampal PV-INs exhibited learning-associated sustained activity at the early stage of tEBC acquisition. Moreover, the PV-IN sustained activity was positively correlated with the occurrence of conditioned eyeblink responses at the early learning stage. Suppression of the PV-IN sustained activity impaired the acquisition of tEBC, whereas the PV-IN activity suppression had no effect on the acquisition of delay eyeblink conditioning, a hippocampus-independent learning task. Learning-associated augmentation in the excitatory pyramidal cell-to-PVIN drive may contribute to the formation of PV-IN sustained activity. Suppression of the PV-IN sustained activity disrupted hippocampal gamma but not theta band oscillation during the CS-US interval period. Gamma frequency (40 Hz) activation of the PV-INs during the CS-US interval period facilitated the acquisition of tEBC. Our current findings highlight the involvement of hippocampal PV-INs in tEBC acquisition and reveal insights into the PV-IN activity kinetics which are of key importance for the hippocampal involvement in associative learning.

Key words: associative learning; hippocampus; interneuron; mouse; multichannel recording; trace conditioning

Significance Statement

The cellular mechanisms underlying associative learning have not been fully clarified. Previous studies focused on the involvement of hippocampal pyramidal cells in associative learning, whereas the activity and function of hippocampal interneurons were largely neglected. We herein demonstrated the hippocampal PV-INs exhibited learning-associated sustained activity, which was required for the acquisition of tEBC. Furthermore, we showed evidence that the PV-IN sustained activity might have arisen from the learning-associated augmentation in excitatory pyramidal cell-to-PVIN drive and contributed to learning-associated augmentation in gamma band oscillation during tEBC acquisition. Our findings provide more mechanistic understanding of the cellular mechanisms underlying the hippocampal involvement in associative learning.

Received Apr. 30, 2022; revised Aug. 25, 2022; accepted Sep. 23, 2022.

Author contributions: Z.Y., Hao C., and B.H. designed research; R.L., W.Z., J.Z., Hui C., Hao C., and B.H. performed research; R.L., W.Z., J.Z., H.Z., Hui C., Hao C., and B.H. analyzed data; H.Z. contributed unpublished reagents/analytic tools; Hao C., Z.Y., and B.H. wrote the paper.

This work was supported by Natural Science Foundation of China Grants 81871039 to Hao C. and 82101561 to J.Z., Open Project Program of Brain and Intelligence Research Key Laboratory of Chongqing Education Commission Grant BIR2019001 to Hao C., Special Project on Improving Scientific and Technological Innovation Ability of Army Medical University Grant 2020XQN01 to Hao C., and Foundation for Innovative Research Groups of the National Natural Science Foundation of China Grant 31921003 to Z.H.

*R.L., W.Z., and J.Z. contributed equally to this work.

The authors declare no competing financial interests.

Correspondence should be addressed to Bo Hu at bohu@tmmu.edu.cn or Hao Chen at haochen@tmmu.edu.cn.

<https://doi.org/10.1523/JNEUROSCI.0834-22.2022>

Copyright © 2022 the authors

Introduction

Learning to associate two events that occur separately in time is a critical function of brain networks (Pilkew and Takehara-Nishiuchi, 2018). Among the networks, the hippocampus is believed to be a key structure as lesion of the dorsal hippocampus produces profound deficits in associative learning (Solomon et al., 1986; Moyer et al., 1990; Weiss et al., 1999; Tseng et al., 2004).

By performing multichannel recordings in the dorsal hippocampus, researchers have found that a sizable proportion of hippocampal pyramidal (PYR) cells display sustained activity spanning the time gap between time-separated stimuli

(McEchron and Disterhoft, 1997; Hattori et al., 2015; Klee et al., 2021). In addition, calcium imaging studies have revealed that a number of hippocampal PYRs can exhibit sequential firing activity in the time gap between time-separated stimuli (Modi et al., 2014; Mount et al., 2021). The sustained and/or sequential firing of hippocampal PYRs enables the hippocampus to bridge the time gap between time-separated stimuli, which is hypothesized to support associative learning (Wallenstein et al., 1998; Kitamura et al., 2015; Kitamura, 2017). However, a recent study has shown that disinhibition of the hippocampal PYRs lead to great sustained activity but impairment in associative learning (Zhang et al., 2021). Likewise, overactivity of hippocampal PYRs has been demonstrated to produce adverse effects on associative learning (Koh et al., 2016). These findings indicate that additional mechanisms beyond the hippocampal PYR activity may be involved in associative learning.

Trace eyeblink conditioning (tEBC) is a hippocampus-dependent associative learning task (Weiss and Disterhoft, 2011), which requires time-separated presentations of a conditioned stimulus (CS) and a reinforcing unconditioned stimulus (US). Recently it has been demonstrated that a number of hippocampal interneurons show increased firing responses to the CS presentations, and optogenetic suppression of the increased firing of hippocampal interneurons impairs the acquisition of tEBC (Zhang et al., 2021). Moreover, there is an increase in the intrinsic excitability of hippocampal interneurons after tEBC training (McKay et al., 2013). Along this line, genetic elimination of γ CamKII subunit in the hippocampal interneurons reduced the ability to learn associative fear responses in mice (He et al., 2021). These findings indicate a critical involvement of hippocampal interneurons in associative learning. Considering the diversity of hippocampal interneurons, however, the question remains about the role of distinct subtype of hippocampal interneurons in associative learning.

The parvalbumin (PV)-expressing cells consist of the largest proportion of interneurons in the dorsal hippocampus (Pelkey et al., 2017). It has been demonstrated that the hippocampal PV interneurons (PV-INs) receive strong excitatory inputs from the PYRs (Gulyás et al., 1993; English et al., 2017); and vice versa, the hippocampal PV-INs innervate the soma and proximal dendrites and strongly control the outputs of neighboring PYRs (Hu et al., 2014; Amilhon et al., 2015). Consequently, the PV-INs are in a good position to interact with the PYRs to influence hippocampal oscillatory states (e.g., theta and gamma band oscillation; Antonoudiou et al., 2020; Strüber et al., 2022), which are highly correlated with associative learning (Shearkhani and Takehara-Nishiuchi, 2013; Nokia and Wikgren, 2014). Accordingly, the dysfunction of PYR-to-PVIN interaction has been associated with impairment in learning associative fear responses (Fuchs et al., 2007; He et al., 2021). The above evidence indicates that the PV-IN is a candidate subtype of hippocampal interneuron critically involved in associative learning. Yet it remains unclear how the hippocampal PV-INs respond to time-separated stimuli and how they interact with the neighboring PYRs to support associative learning.

To address these issues, we measured and manipulated the firing activity of hippocampal PV-INs in mice during a tEBC task. Our results establish a causal relationship between the learning-associated hippocampal PV-IN sustained activity with the acquisition of tEBC. Moreover, our results shed new light on how the hippocampal PV-IN sustained activity supports the acquisition of tEBC.

Materials and Methods

Subjects

All experiments were approved by the Animal Care Committee of Army Medical University and followed the National Institutes of Health *Guide for the Care and Use of Laboratory Animals*. Mice were purchased from The Jackson Laboratory and maintained in the C57BL/6J background ($n = 70$, 3–5 months old, both sexes). The following genotypes of mice were used: PV-Cre (B6.129p2-Pvalb^{tm1(cre)Arbr/J}, stock #017320) and Ai40D (stock #021188). Before the experiment and between the recording sessions, mice were individually housed under a 12 h light/dark cycle with lights on at 8:00 A.M. All experiments were conducted during the light phase of the cycle.

Surgical procedures for multichannel recording and optical fiber implant

The mice were positioned in a brain stereotaxic apparatus under isoflurane anesthesia. A pair of stainless steel wires (bare diameter, 76 μ m; insulated diameter, 140 μ m; catalog #791000, A-M. Systems) were subcutaneously passed through the left upper orbicularis oculi muscle (OOM). A craniotomy was performed in the skull above the hippocampus. With the help of a stereotaxic arm, a diode-tetrode assembly was implanted into the area above the left dorsal hippocampus at the following coordinates (AP, -1.9 mm, ML, -1.6 mm, DV, -0.8 mm relative to the bregma). Fabrication of the diode-tetrode assembly has been previously described in detail (Zhang et al., 2019). Briefly, a 200 μ m optic fiber (catalog #FT200EMT, Thorlabs) was combined with the tetrode array. The laser power was measured with an optical power meter (catalog #PM100D, Thorlabs) before the surgery. Two stainless steel screws were secured to the skull above the cerebellum to serve as ground and reference, respectively. Screws and headstage were fixed in place using C&B Metabond luting cement (Parkell) and dental cement. Low-viscosity silicone (Kwik-Cast, World Precision Instruments) was applied to cover the craniotomy. The mice recovered in their home cage for 1 week before further experimental manipulation. During the recovery, the diode-tetrode assembly was moved down (~ 35 μ m/d) until it reached the pyramidal cell layer characterized by large-amplitude sharp wave ripples (SWRs).

To optogenetically manipulate the activity of hippocampal PV-INs during tEBC training, two optical fibers (catalog #FT200EMT, Thorlabs) were implanted into bilateral dorsal hippocampus (AP, -1.9 mm, ML, ± 1.6 mm, DV, -1.0 mm) of virus-injected PV-Cre mice. The fiber implantation was performed 3–4 weeks after viral injection. After the surgery, the mice were individually housed and were allowed to recover for 1 week.

Stereotaxic virus injection for behavioral test

We injected adeno-associated virus (AAV)2-CAG-FLEX-ArchT-GFP for neuronal inhibition, AAV2-Ef1a-DIO-ChR2(h134R)-mCherry for neuronal activation, and AAV2-Ef1a-DIO-EGFP or AAV2-Ef1a-DIO-mCherry for control. The virus was obtained from OBiO and was injected into bilateral dorsal hippocampus of PV-Cre mice according to the mouse brain atlas (Franklin and Paxinos, 2008). The virus was injected by a Nanoject III injector (Drummond Scientific). The coordinates and volumes for virus injection in bilateral dorsal hippocampus were as follows: sites 1 and 2, bregma, AP -1.9 mm, ML ± 1.25 mm, DV -1.10 mm, volume, 140 nl per site; sites 3 and 4, bregma, AP -1.9 mm, ML ± 1.75 mm, DV -1.25 mm, volume, 140 nl per site.

Eyeblink conditioning experiments

Following post-surgery recovery, the mice were habituated to the experimental chamber and preamplifier plug-in manipulation for 2 d. During the habituation, the mice could freely move in a light- and sound-attenuated chamber.

Following habituation, the mice ($n = 86$) received tEBC training for 5 consecutive days. The CS was a 150 ms blue light, which was delivered by an LED mounted on the headstage. The US was a 100 ms cornea air puff, which was delivered via a blunted 27 gauge needle placed ~ 5 mm away from the left eye. A CS was followed by a US with a 250 ms trace interval. The daily training consisted of 100 CS-US paired presentation trials with an average intertrial interval of 23 s (randomly varied between

18 and 28 s). Pseudo-conditioned mice ($n = 8$) received 100 CSs and 100 USs per training day (mean intertrial interval = 11.5 s), but the two stimuli were explicitly unpaired (referred to as unpaired training group).

To evaluate the involvement of hippocampal PV-IN activity in the delay paradigm of eyeblink conditioning (dEBC), 14 mice received CS-US paired presentation training trials in which a 500 ms CS preceded and coterminated with a 100 ms US. Daily dEBC training consisted of 100 CS-US paired presentation trials with an average intertrial interval of 23 s.

Optogenetic manipulation

To optogenetically identify hippocampal PV-INs *in vivo*, a green laser diode (catalog #PL520B, Osram) was activated by a pulse current (120–150 mA) from a laser diode controller (catalog #LDC-205C, Thorlabs). Optogenetic stimulation was applied through the diode-tetrode assembly implanted in PV-Cre mice. One hundred pulses of green light flashes (520 nm in wavelength, 300 ms in duration, 10–15 mW/mm² measured at fiber tip) were delivered when the mice were undergoing pretraining sleep. The interstimulation interval varied from 10 to 20 s with a mean value of 15 s.

To optogenetically inhibit hippocampal PV-IN activity during the CS-US interval period, green laser flashes (520 nm in wavelength, 400 ms in duration, 15 mW/mm²) were delivered at CS onset in each conditioning training trial. To inhibit hippocampal PV-IN activity during the CS presentation period, green laser flashes (520 nm in wavelength, 150 ms in duration, 10 mW/mm²) were delivered at CS onset in each training trial. To inhibit hippocampal PV-IN activity during the trace interval period, green laser flashes (520 nm in wavelength, 250 ms in duration, 15 mW/mm²) were delivered at CS offset in each training trial.

To optogenetically activate hippocampal PV-INs with 40 Hz frequency during the CS-US interval period in PV^{ChR2} mice, blue laser flashes (450 nm in wavelength, 10 ms laser on and 15 ms laser off, 400 ms in duration, 8–10 mW/mm² duration, emitted by blue laser diodes (catalog #PL450B, Osram) were delivered at CS onset in each conditioning training trial. PV^{mCherry} control mice also received 40 Hz blue laser stimulation at CS onset in each conditioning training trial.

In vivo multichannel recording. As we reported previously (Qin et al., 2018; Chen et al., 2021), the multiple unit signals were amplified, digitized at 2,000 Hz using a multiplexed preamplifier (catalog #C3335, Intan Technologies) connected to an electrophysiological signal acquisition board (catalog #RHD2000, Intan Technologies) and stored for off-line analysis. The wideband signal was resampled to 1250 Hz and used as the local field potential (LFP). The differentiated EMG signals were amplified 1000 times and 150–1000 Hz bandpass filtered. Both the CS and the EMG signals were fed into the digital input ports of an acquisition board (catalog #RHD2000, Intan Technologies). Data were visualized by NeuroScope software (<http://neurosuite.sourceforge.net/>; Hazan et al., 2006).

Data analysis

Eyeblinks. The EMG activity of the orbicularis oculi muscle was rectified and integrated with a 1 ms time constant. For each trial, EMG activity was quantified for the baseline period (1–350 ms before CS onset) across 100 daily trials. The baseline EMG activities were averaged, and the SD was calculated. The average value plus four times the SD was defined as the threshold. Each trial with the maximum baseline EMG activity exceeding the threshold was defined as an invalid trial. The eyeblink conditioned response (CR; 51–400 ms after CS onset) and eyeblink unconditioned response (UR; 1–350 ms after US onset) were exclusively measured in the valid trials. A significant eyeblink response was defined as exceeding the average baseline by 4 SDs of the baseline activity for a minimum of 25 ms duration. Any significant eyeblink response during the periods mentioned above was counted as a CR or a UR, respectively (Zhang et al., 2022).

Spike detection and sorting. The spikes were extracted from band-pass-filtered (600–6000 Hz) signals, and their waveforms were projected onto a common basis obtained by principal component analysis of the filtered data (Zhang et al., 2020). Single-unit spikes were isolated off-line using both semiautomatic clustering with KlustaKwik (<http://klustakwik.sourceforge.net/>; Harris et al., 2000) and manual clustering with Klusters

(<http://neurosuite.sourceforge.net/>; Hazan et al., 2006). A cluster was considered a putative single unit if it was well isolated (confirmed by the existence of a 2 ms refractory period devoid of spikes in the autocorrelogram), had a signal-to-noise ratio, and its spike waveforms remained stable throughout the course of the recording (Hattori et al., 2015).

Unit classification. Previous studies have demonstrated that the hippocampal PYRs can be identified versus INs based on a cutoff average firing rate, ranging from 5 to 10 Hz (McEchron and Disterhoft, 1997; McEchron et al., 2001; Csicsvari et al., 1999; Hattori et al., 2015; Witton et al., 2016). In this study, units with a mean overall firing rate <6 Hz and a valley-to-peak spike width >0.35 ms were classified as putative hippocampal PYRs, whereas units with an overall firing rate ≥6 Hz and a valley-to-peak spike width ≤0.35 ms were classified as putative hippocampal INs (Li et al., 2022). Using these criteria, we sorted 1284 putative PYRs and 198 putative INs in the dorsal hippocampus from 16 mice. The proportions of putative PYRs and INs are consistent with previous reports about the cellular composition in the hippocampus (Pelkey et al., 2017).

In vivo PV-IN identification. For each unit, the spikes observed during each laser stimulation trial were assigned to a series of 50 ms time bins 1 s before (baseline period) and 1 s after the green laser onset. To identify the PV-INs, the firing rates of all putative INs were normalized according to their baseline firing rates as follows:

$$FR = 100\% \times (FR_{\#bin} - \text{mean}FR_{\text{Baseline}}) / \text{mean}(FR_{\text{Baseline}}),$$

where #bin refers to arbitrary time bin. This response mapping procedure allowed us to compare the firing rate of each unit before (1 s before each CS onset) and during the green light pulses (300 ms intervals starting from each stimulation onset). An IN unit was identified as the PV-IN if its firing activity was reliably suppressed (<50% baseline level) by green laser stimulations with short latency (<5 ms). The PV-INs were further confirmed by their firing phases in sharp wave ripples and theta oscillations (Lapray et al., 2012).

Neuronal activity during EBC. For each hippocampal unit, the spikes observed during each valid trial were assigned to a series of 50 ms time bins 1 s before (baseline period) and 1 s after the CS onset. The average number of spikes observed for 20 bins before the CS onset was used as the baseline activity for that trial. For each time bin (three bins during the CS and five bins during the trace interval), a significant change of spike activity was determined by a series of paired *t* tests between the number of spikes observed for that bin and the baseline period. Bonferroni corrections were conducted to control for multiple comparisons. The firing rate (FR) of each bin was normalized as follows:

$$Z = (FR_{\#bin} - \text{mean}FR_{\text{Baseline}}) / \text{s.d.}(FR_{\text{Baseline}}),$$

where #bin refers to arbitrary time bin. Increases in spike activity were considered significant if they differed from the normalized basal firing levels by >2 SDs ($Z > 2$) of the normalized basal firing rates.

Quantification of fast excitatory drive from PYRs onto PV-INs. In this study we focused our analysis on the units recording from the same tetrode. The local fast excitatory drive from PYRs onto PV-INs was identified by a short-latency peak in a cross-correlogram (CCG) between the PYR and the PV-IN spiking responses (Barthó et al., 2004). A peak in a CCG was defined as significant when at least one of the bins exceeded the 99th percentile of the mean. The mean (control number of spikes) was calculated between −50 and −10 ms to control for a potential low-frequency fluctuation of firing rate. Normalized CCG was obtained by dividing the observed CCG by the expected number of spikes per bin. The expected number of spikes per bin could be estimated by the PV-IN average firing rate. The CCG data were averaged across all PYR/PV-IN pairs recorded in the same tetrodes. Significant peaks (1 ms bin width) within 3 ms of the center bin were used to assess the fast PYR-to-PV-IN drive strength (English et al., 2017).

Quantification of CS-evoked changes in oscillatory amplitude. To examine CS-evoked changes in oscillatory amplitude, the Hilbert transform was used to calculate the instantaneous amplitude of specific

frequency bands. Theta (5–12 Hz) and gamma (35–85 Hz) bands were examined. The quantification procedures have been introduced by Tanninen et al. (2017). First, in each trial, raw LFP signals during a 2 s window around CS onset were filtered with a bandpass filter (third-order Chebyshev type 1, forward and backward for zero-phase distortion). Second, the instantaneous amplitude was calculated as the absolute value of the Hilbert transform of the filtered signal. Third, the amplitude was divided by the averaged amplitude during a 400 ms window before the CS onset. Fourth, the normalized amplitude was averaged during the time 1–400 ms from CS onset. Similar procedures were used to quantify the oscillatory amplitude in either baseline or US periods. The time window for baseline period analysis was 1–400 ms before the CS onset, whereas the time window for US period analysis was 1–400 ms after the US onset.

Histologic verification

To visualize the recording sites in PV^{ArchT} mice ($n = 16$), electrolytic lesions (30 μ A for 10 s, DC current) were made at the end of all behavioral and recording experiments. Two days later, the mice were anesthetized with pentobarbital (100 mg/kg, i.p.) and perfused with ice-cold saline and 4% paraformaldehyde (PFA; prepared in 0.1 M phosphate buffer, pH 7.4). The brain was removed and postfixed in 4% PFA for 24 h. Thereafter, the brain was dehydrated in a 30% sucrose solution for 48 h. Coronal sections (40 μ m thick) were cut on a freezing microtome (model CM1900, Leica) and collected in PBS (0.01 M, pH 7.4) for later staining. After three washes (5 min each), the sections containing the dorsal hippocampus were mounted in Fluoromount medium with DAPI fluorescence (catalog #F6057, Sigma-Aldrich). The tip placements of tetrodes were checked by a fluorescence microscope (model BX53, Olympus).

Ninety-two virus-injected PV-Cre mice were transcardially perfused immediately following optogenetic experiments to confirm viral expression and optical fiber implantation position. Coronal slices (40 μ m in thickness) were obtained using the same procedure mentioned above. The slices of PV-Cre mice were prepared for 1 h of permeabilization with 0.5% Triton X-100 in PBS followed by 1 h of block with 5% BSA. Slices were incubated with primary antibody (parvalbumin, 1:400; catalog # 11427, Abcam) overnight at 4°C and secondary antibody (AlexaFluor 568, 1:800; catalog #A10042, Invitrogen) were incubated for 2 h at room temperature. Nuclei were stained with DAPI. Fluorescence images were taken by a confocal laser-scanning microscope (IXplore SpinSR, Olympus).

Statistics

Data are expressed as the mean \pm SEM unless otherwise noted. The statistical significance for behavioral analysis was determined by one-way or two-way ANOVAs with repeated measures as needed. Difference in firing activity between two groups (paired vs unpaired) was determined by independent t test (two tailed). Paired t tests were used to determine the difference in firing activity between two states (CR vs no CR) and the effect of optogenetic manipulation on the CR performance. A value of $p < 0.05$ was significant for all tests. Significance levels of data were denoted as * $p < 0.05$, ** $p < 0.01$ and *** $p < 0.001$; $p > 0.05$ was insignificant and was denoted as n.s.

Results

Optogenetic identification of hippocampal PV-INs *in vivo*

To achieve specific identification and manipulation of PV-INs *in vivo*, we selectively expressed the light-activated inhibitory proton pump (ArchT) in the PV-INs by crossing PV-Cre mice with mice expressing cre-dependent ArchT (Ai40D). We first performed immunohistological experiments to assess the efficiency and specificity of ArchT expression in the hippocampus of heterozygote PV^{ArchT} mice (Fig. 1A). The results showed that $82.4 \pm 2.3\%$ of PV-INs expressed ArchT in the dorsal hippocampus of PV^{ArchT} mice, along with high-level expression specificity ($90.7 \pm 1.6\%$, averaged from 8 PV^{ArchT} mice). As shown by the

example recording traces from a PV^{ArchT} mouse in Figure 1B, the delivery of green laser pulses (10–15 mW/mm² light intensity, 300 ms duration, 10–30 s intervals) produced significant suppression in firing activity of a hippocampal PV-IN. We referred to those units showing significantly suppressive responses ($>50\%$ in firing suppression) that were time locked to green laser stimulation as the optogenetically tagged PV-INs ($p < 0.01$, permutation test, laser on vs laser off baseline). With this opto-tagging method, we identified 106 dorsal hippocampal PV-INs ($72.7 \pm 1.5\%$ in firing suppression averaged from 106 units in 16 PV^{ArchT} mice; Fig. 1C) which exhibited high firing rate (13.6 ± 0.8 Hz) and narrow valley-to-peak spike width (0.27 ± 0.01 ms averaged from 106 units; Fig. 1D). The optogenetically identified PV-INs increased their firing during the hippocampal SWRs (Fig. 1E,F) and preferred to emit their spikes at the ascending phase of SWRs ($205.0 \pm 9.9^\circ$ with 0° at the peak, $n = 106$; Fig. 1G). In addition, the optogenetically identified PV-INs emitted more spikes at the descending phase of theta oscillations ($166.3 \pm 16.5^\circ$ with 0° at the peak, $n = 106$; Fig. 1H,I). The firing characteristics of optogenetically identified PV-INs are consistent with the previous findings reported for hippocampal PV-INs (Klausberger et al., 2003; Lapray et al., 2012). We thus established a reliable approach to identify hippocampal PV-INs and manipulate their firing activity *in vivo*.

Learning-associated sustained activity in hippocampal PV-INs

Having optogenetically identified the hippocampal PV-INs, we next sought to investigate whether and how these interneurons change their firing activities during learning an associative sensorimotor behavior. For this purpose, we trained the freely moving mice to learn a tEBC task in which a light CS was paired with an air puff US (Fig. 2A). To avoid the aversive USs, the mice responded to the light CSs and lowered their upper eyelids just before the presentation of the air puff USs (Fig. 2B,C). We found that the mice receiving CS-US paired presentations showed fewer CRs on days 1–2 (CR incidence, $39.7 \pm 7.0\%$) and more CRs on days 4–5 (CR incidence, $61.5 \pm 9.3\%$; within-group effect, $F_{(4,28)} = 3.327$, $p = 0.024$, $n = 8$, one-way ANOVA with repeated measures; Fig. 2B). Across five training days, the paired training mice exhibited a significantly higher CR level than the unpaired training mice (CR incidence, between-group effect, $F_{(1,14)} = 34.064$, $p < 0.001$; training days times group interaction, $F_{(4,56)} = 1.920$, $p = 0.120$; CR peak amplitude, between-group effect, $F_{(1,14)} = 5.512$, $p = 0.034$; training days times group interaction, $F_{(4,56)} = 1.230$, $p = 0.309$; $n = 8$ for both paired and unpaired training mice, two-way ANOVAs with repeated measures; Fig. 2B–D). These results suggested that the paired training mice learned the CS-US association across five training days. Based on the CR level in paired training mice, we further separated behavioral training into two stages, the early learning stage (ELS; days 1–2) with relatively few CRs and the late-learning stage (LLS; days 4–5) with an asymptotic high CR level (Fig. 2B,C).

Next, we analyzed the firing activity of optogenetically identified hippocampal PV-INs during the acquisition of tEBC (Fig. 3A). For this analysis, we ensured that at least one PV-IN was optogenetically identified in each mouse on each training day (1.44 ± 0.11 PV-INs for paired and 1.41 ± 0.12 PV-INs for unpaired training mice). It was found that presentation of the CS evoked an elevated firing activity in the hippocampal PV-INs (Fig. 3B,C). The CS-evoked PV-IN firing activity did not cease when the CS presentation stopped. Instead, the PV-IN firing activity could span both the CS presentation and trace interval

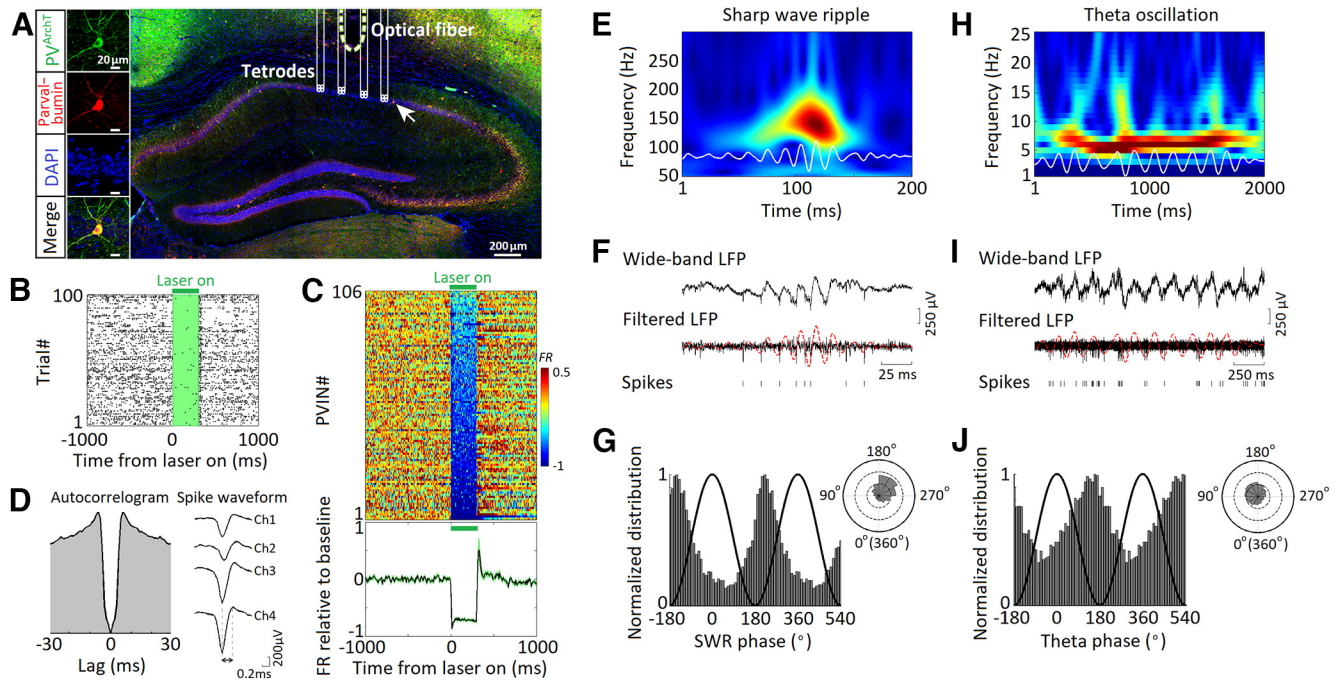


Figure 1. Optogenetic identification of hippocampal PV-INs *in vivo*. **A**, Right, Representative image shows the combination of multichannel recording and optogenetic manipulation in the dorsal hippocampus of a PV^{ArchT} mouse. The PV^{ArchT} mice were obtained by hybridizing PV-Cre mice with Ai40D mice. Scale bar, 200 μ m. Left, Magnification images show the specific labeling of ArchT-EGFP (green) in PV-INs (red). Scale bar, 20 μ m. **B**, Raster plot illustrates the firing responses of an identified hippocampal PV-IN to 300 ms green laser stimulations. Note that there was an obvious suppression of PV-IN firing activity time locked to green laser stimulation. **C**, Top, Pseudo-colored peristimulus time histograms (PSTHs) of all identified PV-INs ($n = 106$ from 16 PV^{ArchT} mice). Each row represents one identified PV-IN. Darker shades represent decrease in firing activity. Bottom, Population-averaged PSTH for all identified PV-INs ($n = 106$). Shading represents SEM. **D**, Autocorrelogram and spike waveform of an identified PV-IN illustrated in **B**. Calibration: 200 μ V for spike amplitude or 0.2 ms for spike width. **E**, Power spectrogram map shows a representative SWR event in the dorsal hippocampus. The SWR event is illustrated and highlighted in red. Band-filtered (100–250 Hz) LFP trace is depicted in white. **F**, Top, Wide-band hippocampal LFP trace listed in **E**. Bottom, High-pass filtered (>600 Hz) LFP trace shows the spikes of an identified PV-IN. Each detected spike is indicated by a black tick. Band-filtered (100–250 Hz) LFP trace is superimposed in red dashed line. Calibration: 250 μ V for LFP amplitude or 25 ms for time. **G**, Distribution of preferred firing phase of the identified PV-IN (listed in **F**) to the SWR oscillation. Black line indicates two consecutive SWR cycles. Note that the identified PV-IN preferred to fire at the ascending phase (180–270°) of SWR oscillation. Inset, Polar histogram showing spike phase of the identified PV-IN to SWR oscillation. **H**, Power spectrogram map shows a representative theta oscillation event in the dorsal hippocampus. The theta oscillation was illustrated and highlighted in red. Band-filtered (5–12 Hz) LFP trace is depicted in white. **I**, Top, Wide-band hippocampal LFP trace listed in **H**. Bottom, High-pass filtered (>600 Hz) LFP trace shows the spikes of an identified PV-IN. Each detected spike is indicated by a black tick. Band-filtered (5–12 Hz) LFP trace was superimposed in red dashed line. Calibration: 250 μ V for LFP amplitude or 250 ms for time. **J**, Distribution of preferred firing phase of the identified PV-IN (listed in **I**) to theta oscillation. Black line indicates two consecutive theta cycles. Note that the identified PV-IN emitted more spikes at the descending phase (90–180°) of theta oscillation. Inset, Polar histogram showing spike phase of the identified PV-IN to theta oscillation.

periods (hereafter referred to as sustained activity in the CS-US interval period; Fig. 3B,C).

At the ELS, the paired training mice showed significantly greater PV-IN sustained activity than the unpaired training mice (Z-scored firing rate, 8.99 ± 1.76 , $n = 23$ for paired vs 3.87 ± 0.50 , $n = 28$ for unpaired training mice, $t_{(49)} = 3.113$, $p = 0.003$, independent t test; Fig. 3D,E). This difference remained significant even when three PV-INs with the most discrete distribution were excluded (Z-scored firing rate, 6.27 ± 0.93 , $n = 20$ for paired vs 3.87 ± 0.50 , $n = 28$ for unpaired training mice, $t_{(46)} = 2.498$, $p = 0.016$, independent t test). In addition, the greater PV-IN sustained activity in paired training mice unlikely arose from their higher baseline firing rates as there was no significant difference in baseline PV-IN firing rates between two groups of mice at the ELS (baseline firing rate, 14.2 ± 1.5 Hz, $n = 23$ for paired vs 12.0 ± 1.9 Hz, $n = 28$ for unpaired training mice, $t_{(49)} = 0.885$, $p = 0.380$, independent t test).

In contrast, the PV-IN sustained activity in paired training mice significantly diminished (Z-scored firing rate, 4.51 ± 0.69 , $n = 23$ at LLS vs 8.99 ± 1.76 , $n = 23$ at ELS, $t_{(44)} = 2.429$, $p = 0.019$, independent t test; Fig. 3D–G) at the LLS and was comparable to that in the unpaired training mice (Z-scored firing rate, 4.51 ± 0.69 , $n = 23$ for paired vs 3.50 ± 0.46 , $n = 17$ for unpaired training mice, $t_{(38)} = 1.168$, $p = 0.250$, independent t test; Fig. 3F,G). In addition, there

was no difference in the baseline firing rate of PV-INs between the paired and unpaired training mice at the LLS (baseline firing rate, 12.3 ± 2.3 Hz, $n = 23$ for paired vs 11.6 ± 1.7 Hz, $n = 17$ for unpaired training mice, $t_{(38)} = 0.257$, $p = 0.798$, independent t test). These results suggest that the hippocampal PV-INs manifest learning-associated sustained activity during the acquisition of tEBC. Of note, the hippocampal PV-IN sustained activity exhibits dynamic change across learning, with greater responses at the ELS.

At the ELS, the paired training mice also showed greater US-evoked PV-IN activity than the unpaired training mice (Z-scored firing rate, 11.80 ± 1.57 , $n = 23$ vs 5.44 ± 1.05 , $n = 28$, $t_{(49)} = 3.549$, $p = 8.653 \times 10^{-4}$, independent t test; Fig. 3E,F). At the LLS, the US-evoked PV-IN activity in paired training mice significantly diminished (Z-scored firing rate, 6.35 ± 1.83 , $n = 23$ at LLS vs 11.80 ± 1.57 , $n = 23$ at ELS, $t_{(44)} = 2.505$, $p = 0.016$, independent t test; Fig. 3E,F,H,I). In contrast, the US-evoked PV-IN activity in the unpaired training mice remained stable across the ELS and the LLS (Z-scored firing rate, 5.44 ± 1.05 , $n = 28$ at ELS vs 5.25 ± 1.17 , $n = 17$ at LLS, $t_{(43)} = 0.122$, $p = 0.904$, independent t test; Fig. 3F,I).

Greater hippocampal PV-IN sustained activity in CR state

To further quantify the association of hippocampal PV-IN sustained activity with CR acquisition, we compared the PV-IN

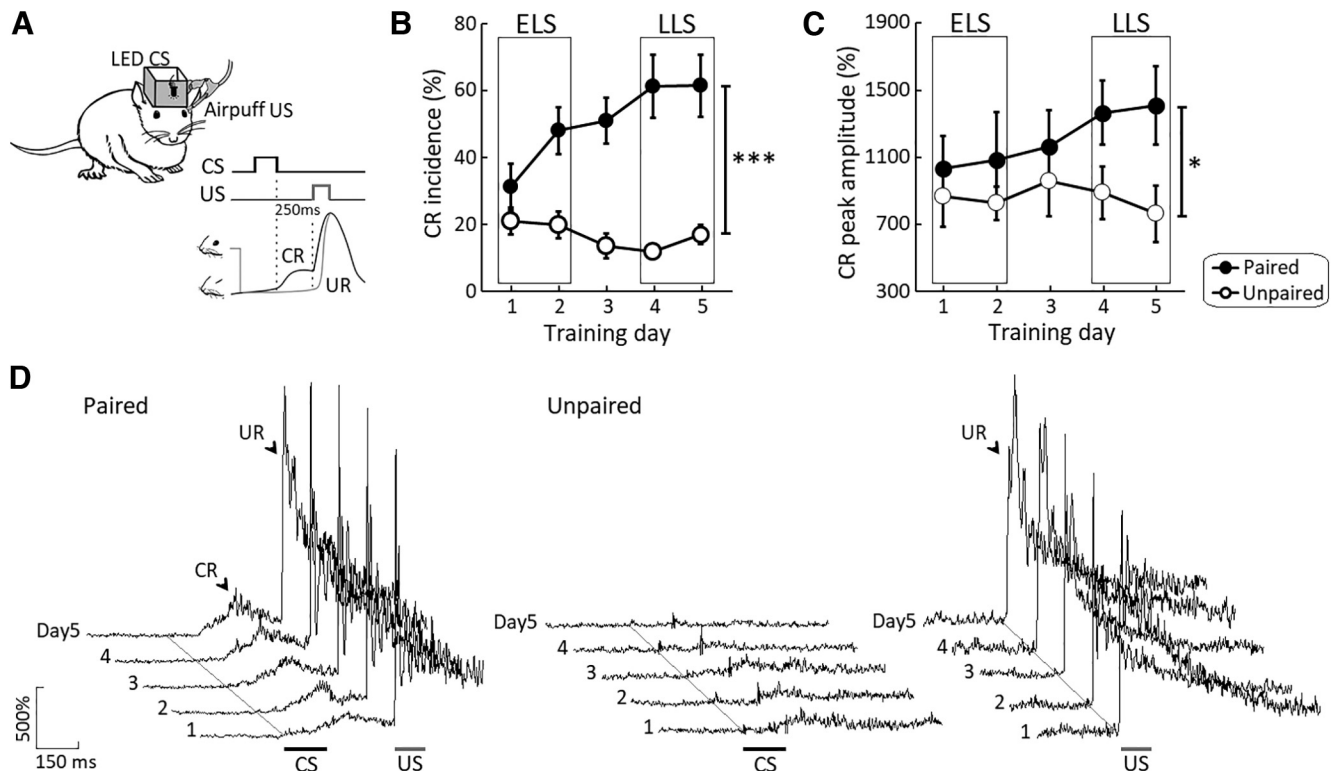


Figure 2. Acquisition of tEBC in freely moving mice. **A**, Experimental setup. Left, Diagram shows the delivery of CS (blue LED light) and US (corneal air puff) in a freely moving mouse. Right, Diagram shows temporal relationship between the CS and the US. **B**, CR incidence measured from the paired ($n = 8$, filled circles) and unpaired ($n = 8$, empty circles) training mice across five training days. **C**, CR peak amplitude measured from the paired ($n = 8$, filled circles) and unpaired ($n = 8$, empty circles) training mice across five training days. **D**, OOM EMG responses across five training days for a representative paired (left) and unpaired (right) training mouse, respectively. The CR and the UR are indicated by black arrows. CS, black bar; US, gray bar. Calibration: 500% for EMG activity or 150 ms for time. Data are presented as mean \pm SEM. *** $p < 0.001$, * $p < 0.05$.

sustained activity between the CR and the no-CR states in paired training mice. It should be noted that three PV-INs were excluded from this analysis because they generated too few spikes to normalize their firing in the no-CR state (one unit at the ELS and two units at the LLS). At the ELS, we found that the PV-IN sustained activity in the CR trials was significantly greater than in the no-CR trials (Z-scored firing rate, 8.50 ± 1.73 for CR trials vs 4.52 ± 0.61 for no-CR trials, $n = 22$, $t_{(21)} = 2.601$, $p = 0.017$, paired t test; Fig. 4A–C). This difference remained significant even when two PV-INs with the most discrete distribution were excluded (Z-scored firing rate, 6.54 ± 1.12 for CR trials vs 4.30 ± 0.64 for no-CR trials, $n = 20$, $t_{(19)} = 2.149$, $p = 0.045$, paired t test). In contrast, no difference in the PV-IN activity was observed during the US period (Z-scored firing rate, 9.41 ± 1.38 for CR trials vs 7.55 ± 0.68 for no-CR trials, $n = 22$, $t_{(21)} = 1.307$, $p = 0.205$, paired t test; Fig. 4D).

At the LLS, there was no difference in PV-IN sustained activity between the CR and no-CR trials (Z-scored firing rate, 3.10 ± 0.49 for CR trials vs 2.62 ± 0.38 for no-CR trials, $n = 21$, $t_{(20)} = 0.964$, $p = 0.346$, paired t test; Fig. 4G). No difference in US-evoked PV-IN activity was found between the CR and no-CR states at the LLS (Z-scored firing rate, 4.07 ± 1.06 for CR trials vs 3.98 ± 0.87 for no-CR trials, $n = 21$, $t_{(20)} = 0.124$, $p = 0.902$, paired t test; Fig. 4H). These results provided further evidence that the PV-IN sustained activity is associated with CR performance at the ELS.

Hippocampal PV-IN sustained activity is required for the acquisition of tEBC

Considering that the hippocampal PV-IN sustained activity was associated with the CR occurrence, we hypothesized that it might

contribute to the acquisition of tEBC. We tested this hypothesis by selectively suppressing the hippocampal PV-IN sustained activity during the acquisition of tEBC. For this purpose, we injected viral vectors encoding ArchT (AAV2-FLEX-ArchT-GFP, PV^{ArchT} , $n = 9$) or an opsin negative control vector (AAV2-Ef1a-DIO-GFP, PV^{GFP} , $n = 7$) into bilateral dorsal hippocampus of PV -Cre mice (Fig. 5A,B). It was shown that optogenetic suppression of hippocampal PV-IN sustained activity produced severe impairments in the CR acquisition (Fig. 5C–E). Two-way mixed ANOVA (suppression times training day) across training days revealed no significant effects in the interaction between suppression and training days (CR incidence, $F_{(4,56)} = 0.282$, $p = 0.888$; CR peak amplitude, $F_{(4,56)} = 0.020$, $p = 0.999$; Fig. 5D, E), but significant suppression effects (CR incidence, $F_{(1,14)} = 12.493$, $p = 0.004$; CR peak amplitude, $F_{(1,14)} = 4.579$, $p = 0.049$; Fig. 5D,E). The behavioral results could not be explained by the disability of PV^{ArchT} mice because they could acquire the CRs across 5 additional days (days 6–10) when there were no green laser stimulations. As illustrated in Figure 5C, a representative PV^{ArchT} mouse exhibited obvious CR improvement across training days 6–10. Statistical analysis revealed that the PV^{ArchT} mice emitted comparable CRs on days 6–10 to those of PV^{GFP} mice on days 1–5 (CR incidence, $F_{(1,14)} = 0.088$, $p = 0.771$; CR peak amplitude, $F_{(1,14)} = 0.061$, $p = 0.999$, two-way ANOVA with repeated measures). These results indicate a requirement of hippocampal PV-IN sustained activity for the acquisition of tEBC.

The PV-IN sustained activity spanned both the CS presentation and the trace interval periods. However, the specific role of hippocampal PV-IN activity during either the CS presentation or the trace interval period remains unclear. To address this issue,

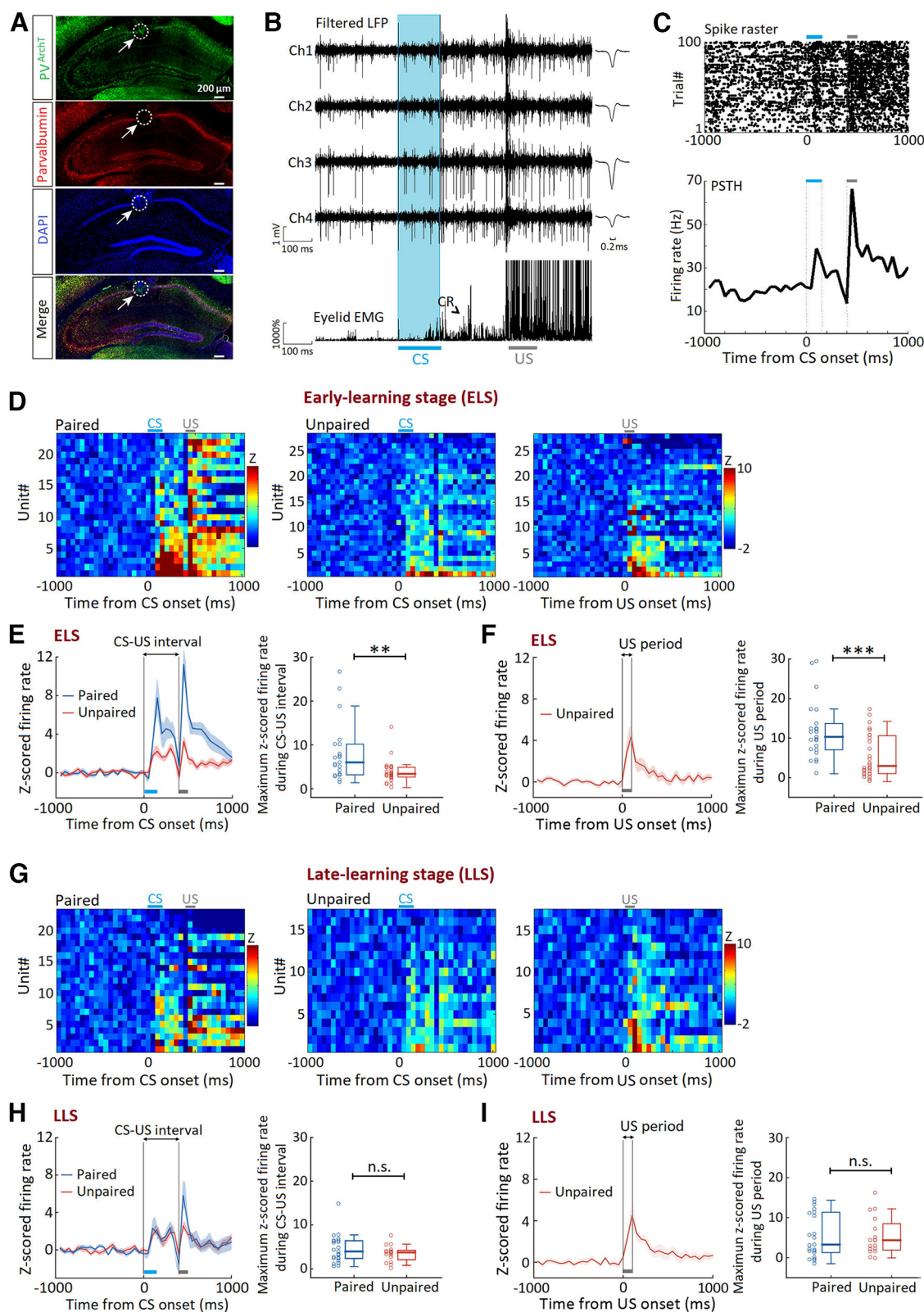


Figure 3. Greater hippocampal PV-IN sustained activity at the early stage of tEB acquisition. **A**, Immunofluorescence image shows a representative tetrode recording site in the dorsal hippocampus of a PV^{ArchT} mouse. **B**, Top, Tetra recording traces show the CS-evoked sustained activity of an optogenetically identified hippocampal PV-IN. Bottom, OOM EMG activity 300 ms before and 700 ms after the CS onset. Calibration: 1 mV for LFP amplitude or 1000% for EMG activity and 100 ms for time. **C**, Raster plot (top) and peristimulus time histograms (PSTHs; bottom) illustrates spiking responses of the hippocampal PV-IN (listed in **B**) to 100 CS-US paired presentations. **D**, Left, Z-scored firing activities of hippocampal PV-INs ($n = 23$) for paired training mice at the ELS. Right, Z-scored firing activities of hippocampal PV-INs ($n = 28$) for unpaired training mice at the ELS. Heat map rows represent Z-score-transformed PSTH for individual hippocampal PV-INs, and columns represent time bins relative to the CS onset or the US onset (50 ms bin width). **E**, Left, Plots show the average Z-scored PV-IN firing activities 1 s before and 1 s after the CS onset for paired (blue, $n = 23$ units) and unpaired (red, $n = 28$ units) training mice at the ELS. Shading represents SEM. Right, Comparison of maximum Z-scored PV-IN activities during the CS-US interval period between the paired (blue) and unpaired (red) training mice. **F**, Left, Plot shows the average Z-scored PV-IN firing activities (red, $n = 28$) 1 s before and 1 s

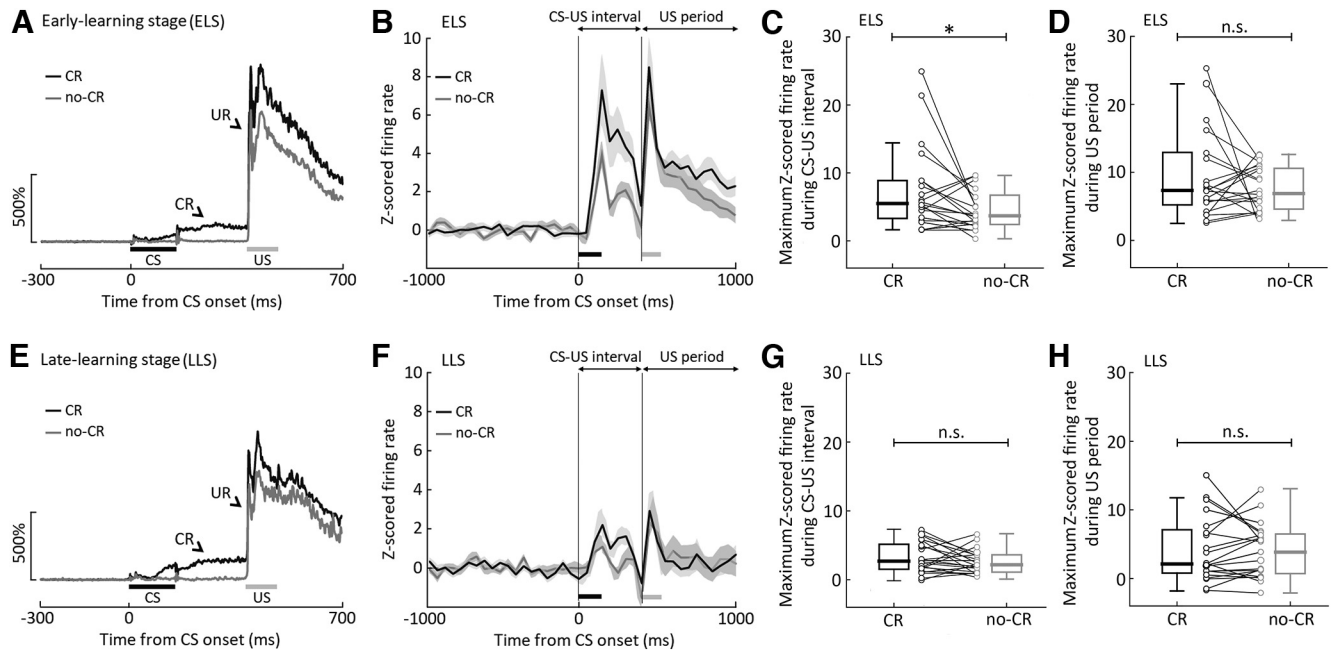


Figure 4. PV-IN sustained activity distinguishes between the CR and no-CR state at the early stage of tEBC acquisition. **A**, CR (black) and no-CR (gray) OOM EMG traces averaged from paired training mice ($n = 8$) at the ELS. Calibration, 500% for EMG activity. **B**, Z-scored firing activities of hippocampal PV-INs ($n = 22$ units) in the CR (black) versus no-CR (gray) trials at the ELS. **C**, At the ELS, CS-evoked PV-IN sustained activity in CR trials was significantly greater than in no-CR trials. **D**, US-evoked PV-IN firing activity in CR trials was comparable to that in no-CR trials. **E**, CR (black) and no-CR (gray) OOM EMG traces averaged from paired training mice ($n = 8$) at the LLS. Calibration, 500% for EMG activity. **F**, Z-scored firing activities of hippocampal PV-INs ($n = 21$ units) in the CR (black) versus no-CR (gray) trials at the LLS. **G**, At the LLS, CS-evoked PV-IN sustained activity in CR trials (black) was comparable to that in no-CR trials (gray). **H**, US-evoked PV-IN firing activity in CR trials (black) was comparable to that in no-CR trials (gray). The CRs and the URs were indicated by black arrows, respectively. CS, black bar; US, gray bar. **C, D, G, H**, Box plots show median \pm IQR, whiskers show range. * $p < 0.05$, n.s. $p > 0.05$.

we applied optogenetic suppression briefly within either the CS presentation or the trace interval period, respectively. Notably, a 150 ms suppression of PV-IN activity during the CS presentation period caused a significant impairment in the CR acquisition (suppression effects, CR incidence, $F_{(1,10)} = 8.670$, $p = 0.015$; CR peak amplitude, $F_{(1,10)} = 4.433$, $p = 0.062$; suppression times training day interaction, CR incidence, $F_{(1,10)} = 0.848$, $p = 0.379$; CR peak amplitude, $F_{(1,10)} = 0.418$, $p = 0.532$; $n = 6$ for both PV^{ArchT} and PV^{GFP} mice, two-way ANOVA with repeated measures; Fig. 5F). Likewise, a 250 ms suppression of PV-IN activity during the trace interval period caused a reduction in the CR acquisition (suppression effects, CR incidence, $F_{(1,10)} = 8.318$, $p = 0.016$; CR peak amplitude, $F_{(1,10)} = 1.708$, $p = 0.220$; suppression times training day interaction, CR incidence, $F_{(1,10)} = 0.094$, $p = 0.765$; CR peak amplitude, $F_{(1,10)} = 0.145$, $p = 0.711$; $n = 6$ for both PV^{ArchT} and PV^{GFP} mice, two-way ANOVA with repeated measures; Fig. 5G). These results suggest that the hippocampal

PV-IN activity during either the CS presentation or the trace interval period are both involved in the CR acquisition.

The PV-IN sustained activity diminished at the LLS, raising a possibility that the diminished PV-IN sustained activity may be an important mechanism that contributes to accelerate learning at this stage. Alternatively, the role of PV-IN sustained activity in learning becomes minimal at the LLS. To test these two possibilities, we suppressed the PV-IN sustained activity when the CRs were well learned at the LLS (i.e., on days 5 and 6; Fig. 5H). It was shown that optogenetic suppression of PV-IN sustained activity produced no significant effects on the CR performance in PV^{ArchT} mice ($n = 5$, CR incidence, $t_{(4)} = -1.826$, $p = 0.142$; CR peak amplitude, $t_{(4)} = -0.698$, $p = 0.523$, paired t tests; Fig. 5H). In addition, there were no significant differences in either the CR incidence or the CR magnitude between the PV^{ArchT} and PV^{GFP} mice at the LLS (CR incidence, $t_{(9)} = -1.118$, $p = 0.265$; CR peak amplitude, $t_{(9)} = -0.231$, $p = 0.823$, $n = 5$ for PV^{ArchT} mice and $n = 6$ for PV^{GFP} mice, independent t tests; Fig. 5H). These results indicate that the requirement of hippocampal PV-IN sustained activity for tEBC is minimal at the LLS.

To further confirm the specific requirement of PV-IN sustained activity in tEBC acquisition, we also evaluated the role of PV-IN activity in the acquisition of delay eyeblink conditioning (dEBC), a forebrain-independent task in rodents (Kotani et al., 2002). To address this issue, we trained the mice to acquire dEBC in which a 500 ms CS preceded and coterminated with a 100 ms US and optogenetically suppressed the hippocampal PV-IN activity with 400 ms green laser stimulation (Fig. 6A). We found that both the PV^{ArchT} and the PV^{GFP} mice exhibited significant improvement in CR level across five training days ($61.7 \pm 8.7\%$, $n = 7$ for PV^{ArchT} and $57.5 \pm 6.4\%$, $n = 7$ for PV^{GFP} mice; Fig. 6B). A two-way mixed ANOVA revealed no significant suppression effect (CR incidence, $F_{(1,12)} = 0.944$, $p = 0.350$; CR peak

after the US onset for unpaired training mice at the ELS. Right, Comparison of maximum Z-scored PV-IN activities during the US period between the paired (left, $n = 23$ units) and unpaired (right, $n = 28$ units) training mice. **G**, Left, Z-scored firing activities of hippocampal PV-INs ($n = 23$) for paired training mice at the LLS. Right, Z-scored firing activities of hippocampal PV-INs ($n = 17$) for unpaired training mice at the LLS. **H**, Left, Plots show the average Z-scored PV-IN firing activities 1 s before and 1 s after the CS onset for paired (blue, $n = 23$ units) and unpaired (red, $n = 17$ units) training mice at the LLS. Shading represents SEM. Right, Comparison of maximum Z-scored PV-IN activities during the CS-US interval period between the paired (blue) and unpaired (red) training mice. **I**, Left, Plot shows the average Z-scored PV-IN firing activities (red, $n = 17$) 1 s before and 1 s after the US onset for unpaired training mice at the LLS. Right, Comparison of maximum Z-scored PV-IN activities during the US period between the paired (left, $n = 23$ units) and unpaired (right, $n = 17$ units) training mice. CS, blue bar; US, gray bar. **E, F, H, I**, Box plots show median \pm IQR, whiskers show range. *** $p < 0.001$, ** $p < 0.01$, n.s. $p > 0.05$.

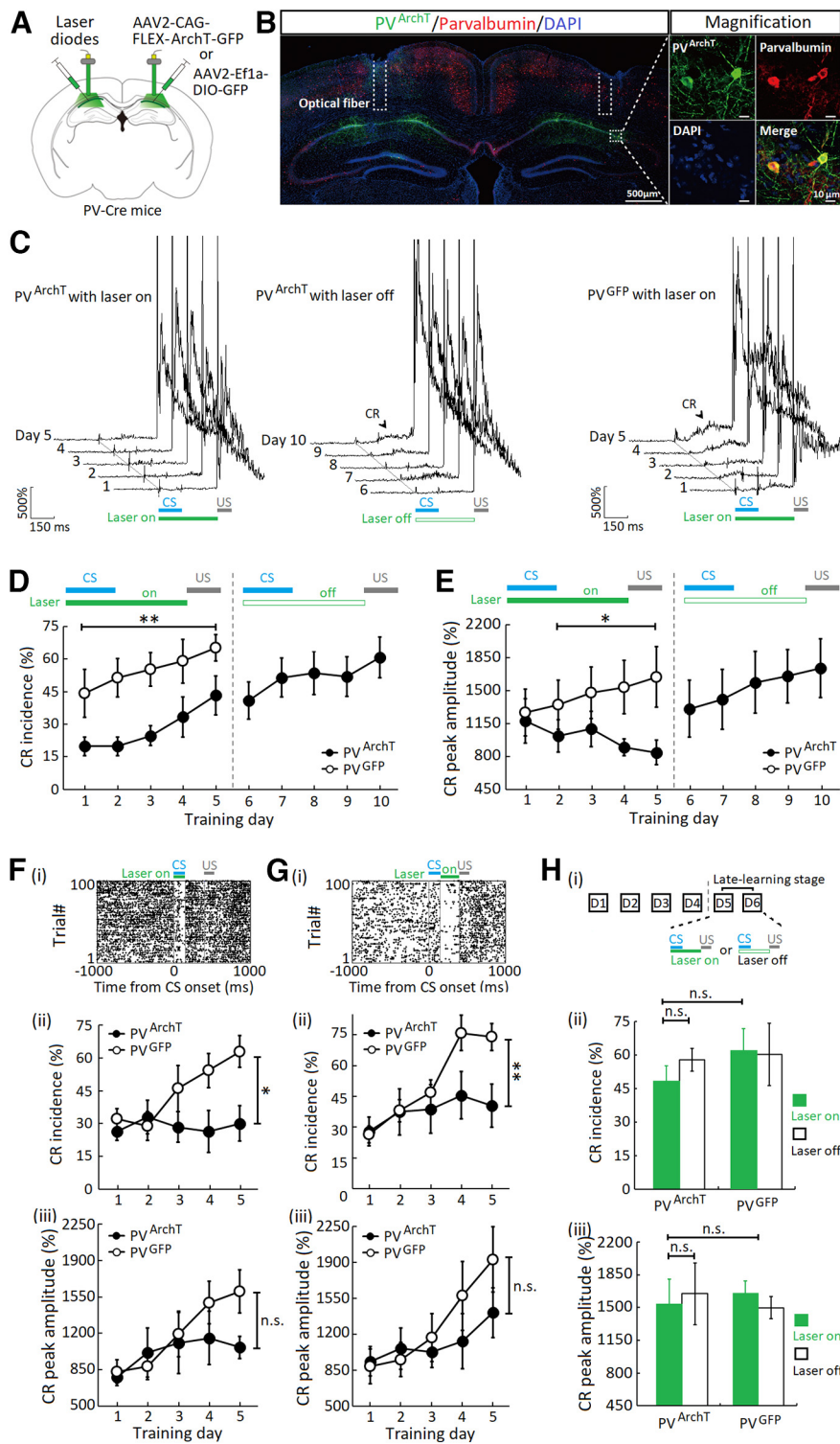


Figure 5. Optogenetic suppression of PV-IN sustained activity impairs the acquisition of tEBC. **A**, Schematic drawing shows optogenetic stimulation in bilateral dorsal hippocampus of PV-Cre mice. **B**, Coronal section of a PV-Cre mouse brain showing ArchT-GFP expression (green) stained with parvalbumin (red) and DAPI (blue) in the dorsal hippocampus. Scale bar, 500 μ m. Insets, Magnification image of GFP expression (green) and parvalbumin immunoreactivity (red). Scale bar, 10 μ m. **C**, Left, OOM EMG responses across 10 training days for a representative PV^{ArchT} mouse. Right, OOM EMG responses across five training days for a representative PV^{GFP} mouse. **D**, CR incidences measured from the PV^{ArchT} (filled circles, $n = 9$) and PV^{GFP} (open circles, $n = 7$) across 10 or 5 training days, respectively. The PV^{ArchT} mice with laser stimulations in the CS-US interval period emitted significantly fewer CRs than those of the PV^{GFP} mice across days 1–5. The PV^{ArchT} mice were able to learn and generate CRs across five additional training days (days 6–10). **E**, CR peak amplitude measured from the PV^{ArchT} (filled circles, $n = 9$) and PV^{GFP} (open circles, $n = 7$) across training days. **F**–**iii**, Raster plot illustrates representative optogenetic suppression of PV-IN activity during the CS presentation period. CR incidence (**ii**) and CR peak amplitude (**iii**) measured from the PV^{ArchT} (filled circles, $n = 6$) and PV^{GFP} mice (open circles, $n = 6$) across five training days. **G**–**iii**, Raster plot illustrates

amplitude, $F_{(1,12)} = 0.183$, $p = 0.677$; Fig. 6B), indicating that the hippocampal PV-IN activity is not required for the acquisition of dEBC.

Learning-associated augmentation in fast excitatory PYR-to-PVIN drive may contribute to PV-IN sustained activity

After establishing the causal relationship between the hippocampal PV-IN sustained activity and the tEBC acquisition, we next explored how the PV-IN sustained activity was formed at the ELS. Considering the sustained PYR firing activity (McEchron and Disterhoft, 1997; Modi et al., 2014; Hattori et al., 2015; Klee et al., 2021; Mount et al., 2021) and strong excitatory-to-inhibitory synapses in the dorsal hippocampus (Gulyás et al., 1993; English et al., 2017), we asked whether the PV-IN sustained activity was, at least in part, because of the excitatory drive from hippocampal PYRs.

To test this, we first analyzed the firing pattern of hippocampal PYRs during the acquisition of tEBC. Based on their firing characteristics, we sorted 738 putative hippocampal PYRs (average firing rate, 1.65 ± 0.05 Hz; valley-to-peak spike width, 0.725 ± 0.004 ms; Fig. 7A,B) from eight paired training mice and 546 putative hippocampal PYRs (average firing rate, 1.55 ± 0.05 Hz; valley-to-peak spike width, 0.736 ± 0.003 ms; Fig. 7A,B) from eight unpaired training mice. At the ELS (days 1–2), it was found that 40% (102/255) of putative hippocampal PYRs showed firing responses during the CS-US interval period in paired training mice, whereas 37.3% (82/220) of putative hippocampal PYRs showed the CS-evoked firing in unpaired training mice (Fig. 7C). In particular, the CS-evoked firing activity of hippocampal PYRs in paired training mice was greater than that of the unpaired training mice (Z-scored firing rate during CS-US interval period, 4.35 ± 0.26 , $n = 102$ units for paired vs 3.23 ± 0.11 , $n = 82$ units for unpaired training mice, $t_{(181)} = 3.692$, $p = 0.0003$, independent t test; Fig. 7D). At

representative optogenetic suppression of PV-IN activity during the trace interval period (**i**). CR incidence (**ii**) and CR peak amplitude (**iii**) measured from the PV^{ArchT} (filled circles, $n = 6$) and PV^{GFP} (open circles, $n = 6$) mice across five training days. **H**–**iii**, Schematic drawing (**i**) shows optogenetic stimulations on hippocampal PV-INs at late-learning stage (days 5 and 6). CR incidence (**ii**) and CR peak amplitude (**iii**) measured from the PV^{ArchT} (green filled bars, $n = 5$) and PV^{GFP} (open bars, $n = 6$) with or without green laser stimulations. CR, black arrow. CS, blue bar; US, gray bar. Data are presented as mean \pm SEM. ** $p < 0.01$, * $p < 0.05$, n.s. $p > 0.05$.

the LLS (days 4–5), however, the CS-evoked firing was comparable between the paired and unpaired training mice (Z-scored firing rate during CS-US interval period, 4.28 ± 0.58 , $n = 114$ units for paired vs 3.53 ± 0.18 , $n = 68$ units for unpaired training mice, $t_{(180)} = 1.168$, $p = 0.2245$, independent t test; Fig. 7E,F). These results suggest that the hippocampal PYRs also exhibit learning-associated firing activities in the CS-US interval at the ELS.

Both the PYRs and the PV-INs showed augmented firing responses during the CS-US interval period, prompting us to further investigating the temporal relationship between their spike activities during tEBC training. In particular, the putative monosynaptic excitatory inputs from the PYRs to PV-INs could be quantitatively estimated by the reliability in which the hippocampal PV-IN fire in the milliseconds after a PYR spike (Csicsvari et al., 1998; Galarreta and Hestrin, 2001; English et al., 2017). As illustrated in Figure 8, A and B, the hippocampal PV-INs in paired training mice tended to have greater reliability to emit spikes immediately after the PYR discharge in the CS-US interval period. Consistent with this, we observed the presence of a sharp peak at short latency (<3 ms after the discharge of the reference PYR) in the PYR-to-PVIN cross-correlation histogram (Fig. 8C), indicating a fast excitatory input from the PYRs onto PV-INs during tEBC training. We then quantified the strength of fast excitatory PYR-to-PVIN drive by measuring the spike transmission probability at the putative monosynaptic peak bins (i.e., ≤ 3 ms) at the ELS and the LLS, respectively. At the ELS (days 1–2), it was revealed that the paired training mice exhibited greater PYR-to-PVIN drive strength than the unpaired training mice (0.074 ± 0.005 , 65 PYR-to-PVIN pairs from eight paired training mice vs 0.058 ± 0.004 , 44 PYR-to-PVIN pairs from eight unpaired training mice, $t_{(14)} = 2.634$, $p = 0.020$, independent t test; Fig. 8C,D). Moreover, the strength of fast excitatory PYR-to-PVIN drive at the ELS was positively correlated with the CR incidence in the paired training mice on day 5 ($r^2 = 0.630$, $p = 0.032$, $n = 8$, Pearson's correlation test; Fig. 8E). In contrast, at the LLS (days 4–5), the paired training mice showed PYR-to-PVIN drive strength comparable to that of the unpaired training mice (0.066 ± 0.005 , 51 PYR-to-PVIN pairs from eight paired training mice vs 0.064 ± 0.007 , 53 PYR-to-PVIN pairs from eight unpaired training mice, $t_{(14)} = 0.190$, $p = 0.852$, independent t test; Fig. 8F,G). In addition, the strength of the fast excitatory PYR-to-PVIN drive seemed to not correlate with CR incidence in the paired training mice on day 5 ($r^2 = 0.078$, $p = 0.503$, $n = 8$, Pearson's correlation test; Fig. 8H). These results suggest that there is learning-associated augmentation in the strength of fast excitatory PYR-to-PVIN drive at the ELS. As both the PYRs and the PV-INs elevated their firing activities during the CS-US interval period, the learning-associated augmentation in fast excitatory PYR-to-PVIN drive effect may, at least in part, contribute to the formation of hippocampal PV-IN sustained activity.

Suppression of PV-IN sustained activity impaired gamma band oscillation during the CS-US interval period

Hippocampal oscillatory activities have been suggested to be strongly influenced by the interaction between the PYRs and

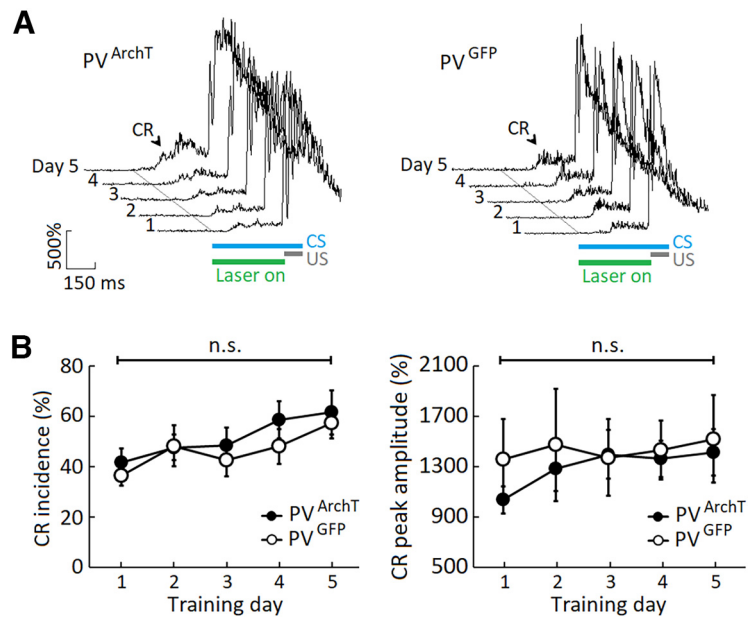


Figure 6. Delay eyeblink conditioning is not blocked by suppression of PV-IN activity. **A**, OOM EMG responses across five training days for a representative PV^{ArchT} (left) and a PV^{GFP} (right) mouse, respectively. CR, black arrow; CS, blue bar; US, gray bar. Calibration: 500% for OOM EMG activity or 150 ms for time. **B**, CR incidence and CR magnitude measured across five training days in PV^{ArchT} (filled circles, $n = 7$) and PV^{GFP} (open circles, $n = 7$) mice. Data are presented as mean \pm SEM. n.s. $p > 0.05$.

PV-INs (Antonoudiou et al., 2020; He et al., 2021). In particular, several types of hippocampal oscillatory activities (e.g., 3–8 Hz theta band and 30–100 Hz gamma band) have been demonstrated to subserve the acquisition of tEBC (Darling et al., 2011; Tanninen et al., 2017). Therefore, we next sought to explore whether and how the PV-IN sustained activity is involved in hippocampal oscillatory activities to support the acquisition of tEBC.

To address this issue, we first tested the effect of suppressing PV-IN sustained activity on the interaction between the hippocampal PYRs and PV-INs (Fig. 9A,B). Considering that both PV-IN sustained activity and PYR-PVIN interaction are greater at the ELS, we focused our analysis and manipulation on training days 1–2. Optogenetic suppression of the PV-IN sustained activity only occupied $\sim 1.67\%$ (100×0.4 s/2400 s) of training time on days 1–2 and produced no significant changes in average firing rates of either the PV-INs (14.175 ± 3.506 Hz averaged from five PV^{ArchT} mice vs 14.814 ± 2.881 Hz averaged from five PV^{GFP} mice, $t_{(8)} = -0.157$, $p = 0.879$, independent t test; Fig. 9C) or the PYRs (2.988 ± 0.604 Hz averaged from five PV^{ArchT} mice vs 2.592 ± 0.138 Hz averaged from five PV^{GFP} mice, $t_{(8)} = 0.715$, $p = 0.405$; Fig. 9D). Nevertheless, selective suppression of the PV-IN sustained activity reduced the possibility that the PV-INs emitted spikes immediately (≤ 3 ms latency) after the PYR discharge during tEBC training (0.0581 ± 0.0034 , $n = 5$ for PV^{ArchT} mice vs 0.0773 ± 0.0031 , $n = 5$ for PV^{GFP} mice, $t_{(8)} = -4.649$, $p = 0.002$, independent t test; Fig. 9A,B,E).

The above results indicate that selective suppression of PV-IN sustained activity is a feasible way to disrupt the interaction between the PYRs and PV-INs at the early stage of tEBC acquisition. Next, we further tested the effect of disrupting PYR-PVIN interaction on hippocampal oscillatory activities at the early stage of tEBC acquisition (Fig. 10A). It was found that the PV^{GFP} mice exhibited a slight but significant increase in the power of gamma

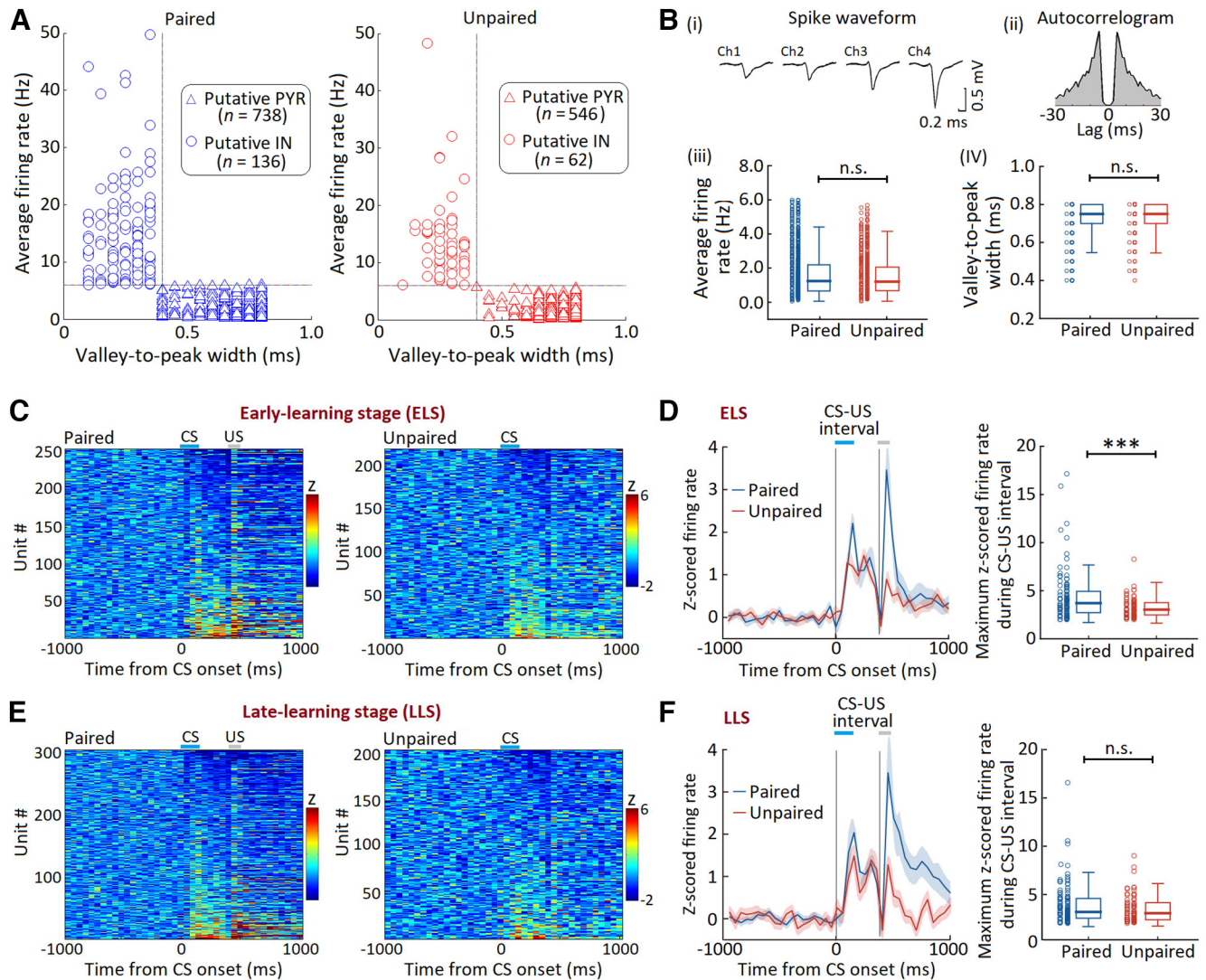


Figure 7. Greater hippocampal PYR activity at the early stage of tEBC acquisition. **A**, Scatter plots of valley-to-peak width of spike waveforms versus average firing rates for 738 and 546 putative hippocampal PYRs isolated from the mice with paired (blue triangles, across 5 d) and unpaired training (red triangles, across 5 d). **Bi–iv**, Spike waveform of a representative hippocampal PYR (**i**) recorded by a tetrode (channels 1–4). Calibration: 500 μ V for spike amplitude or 0.2 ms for spike width. Spike train (**ii**) autocorrelation from the PYR listed in **i**. There are no significant differences in either the average firing rates (**iii**) or the spike width (**iv**) of putative hippocampal PYRs between the paired ($n = 738$, across 8 mice in 5 d) and unpaired training mice ($n = 546$, across 8 mice in 5 d). **C**, Left, Z-scored firing activities of putative hippocampal PYRs ($n = 255$) for paired training mice at the ELS (days 1–2). Right, Z-scored firing activities of putative hippocampal PYRs ($n = 220$) for unpaired training mice at the ELS. Heat map rows represent Z-score-transformed peristimulus time histograms for individual hippocampal PYRs, and columns represent time bins relative to the CS onset (50 ms bin width). **D**, Left, Plots show the average Z-scored PYR firing activities 1 s before and 1 s after the CS onset for paired (blue, $n = 102$ units) and unpaired (red, $n = 82$ units) training mice at the ELS. Shading represents SEM. Right, Comparison of maximum Z-scored PYR activities during the CS-US interval period between the paired (blue) and unpaired (red) training mice. **E**, Left, Z-scored firing activities of putative hippocampal PYRs ($n = 308$) for paired training mice at the LLS (days 4–5). Right, Z-scored firing activities of putative hippocampal PYRs ($n = 210$) for unpaired training mice at the LLS. **F**, Left, Plots show the average Z-scored PYR firing activities 1 s before and 1 s after the CS onset for paired (blue, $n = 114$ units) and unpaired (red, $n = 68$ units) training mice at the LLS. Shading represents SEM. Right, Comparison of maximum Z-scored PYR activities during the CS-US interval period between the paired (blue) and unpaired (red) training mice. CS, blue bar; US, gray bar. **B**, **D**, **F**, Box plots show median \pm IQR, whiskers show range. *** $p < 0.001$, n.s. $p > 0.05$.

band (35–85 Hz) oscillation during the CS-US interval period (relative to baseline period, $8.0 \pm 2.3\%$, $n = 7$, $t_{(6)} = 3.745$, $p = 0.010$, One-sample t test; Fig. 10A,B). In contrast, the PV^{ArchT} mice showed no increase in the power of gamma band (35–85 Hz) oscillation during the CS-US interval period (relative to baseline period, $-1.5 \pm 4.6\%$, $n = 7$, $t_{(6)} = -0.350$, $p = 0.738$, one-sample t test; Fig. 10A,B). The statistical analysis revealed that relative to the PV^{GFP} mice, green laser stimulations significantly inhibited the augmentation of gamma band oscillation during the CS-US interval period in the PV^{ArchT} mice ($-1.5 \pm 4.6\%$, $n = 7$ for PV^{ArchT} mice vs $8.0 \pm 2.3\%$, $n = 7$ for PV^{GFP} mice, $t_{(12)} = -2.218$, $p = 0.047$, independent t test; Fig. 10B). Together, our results suggest that suppression of the PV-IN

sustained activity impaired both the PYR-PVIN interaction and the augmentation of gamma band oscillatory activity in the CS-US interval at the early stage of tEBC acquisition.

However, we did not observe significant changes in the power of theta band (5–12 Hz) oscillation during the CS-US interval period (relative to baseline period, PV^{GFP} mice, $2.5 \pm 8.5\%$, $n = 7$, $t_{(6)} = 0.319$, $p = 0.761$; PV^{ArchT} mice, $18.1 \pm 9.4\%$, $n = 7$, $t_{(6)} = 2.088$, $p = 0.082$; one-sample t test; Fig. 10B). In addition, there was no significant difference in the change of theta band (5–12 Hz) oscillation between the PV^{GFP} and PV^{ArchT} mice during the CS-US interval period ($18.1 \pm 9.4\%$, $n = 7$ for PV^{ArchT} mice vs $2.5 \pm 8.5\%$, $n = 7$ for PV^{GFP} mice, $t_{(12)} = 1.336$, $p = 0.206$, independent t test; Fig. 10B).

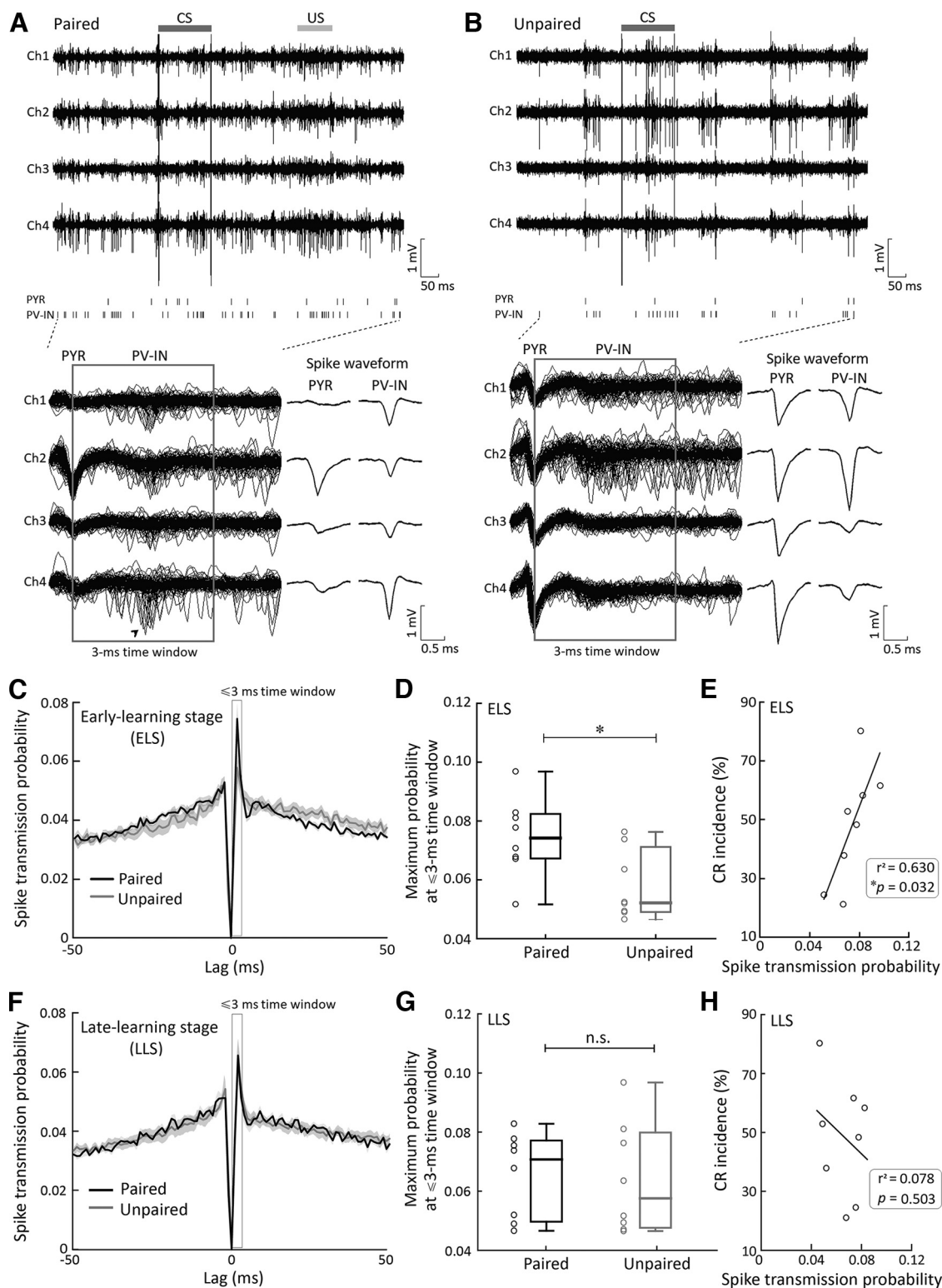


Figure 8. Greater fast excitatory drive from hippocampal PYRs onto PV-INs at the early stage of tEBC acquisition. **A**, Top, Tetrode recording traces show the spiking responses of hippocampal PYR and PV-IN during CS-US paired training. Black ticks represent spikes from single units sorted off-line. Each detected spike was indicated by a black tick. Calibration: 1 mV for LFP amplitude and 50 ms for time. CS, black bar; US, gray bar. Bottom, 1000 randomly sampled traces (filtered at 0.6–6 kHz) aligned to the spikes of the PYR, with the spikes from putative postsynaptic PV-IN. **B**, Top, Tetrode recording traces show the spiking responses of hippocampal PYR and PV-IN during unpaired training. Each detected spike was indicated by a black tick. Calibration: 1 mV for LFP amplitude and 50 ms for time. Bottom, 1000 randomly sampled traces (filtered at 0.6–6 kHz) aligned to the spikes of the PYR, with the spikes from putative postsynaptic PV-IN. **C**, Averaged CCG between PYRs and PV-INs recorded from the paired ($n = 8$, black) and unpaired ($n = 8$, gray) training mice at the ELS. Shading represents SEM. **D**, The spike transmission probability between PYR-PV-IN pairs in paired training mice ($n = 8$, black) was greater than in unpaired training mice ($n = 8$, gray) at the ELS. **E**, Spike transmission probability (≤ 3 ms after the discharge of a reference PYR) at the ELS are plotted against CR incidence (%) for the paired training mice ($n = 8$) on day 5. **F**, CCG between PYRs and PV-INs recorded from the paired ($n = 8$, black) and unpaired ($n = 8$, gray) training mice at the LLS. Shading represents SEM. **G**, The spike transmission probability between PYR-PV-IN pairs in paired training mice ($n = 8$, black) was comparable to the unpaired training mice ($n = 8$, gray). **H**, Spike transmission probability (≤ 3 ms after the discharge of a reference PYR) at the LLS are plotted against CR incidence (%) for the paired training mice ($n = 8$) on day 5. **I**, **J**, Box plots show median \pm IQR, whiskers show range. $*p < 0.05$, n.s. $p > 0.05$.

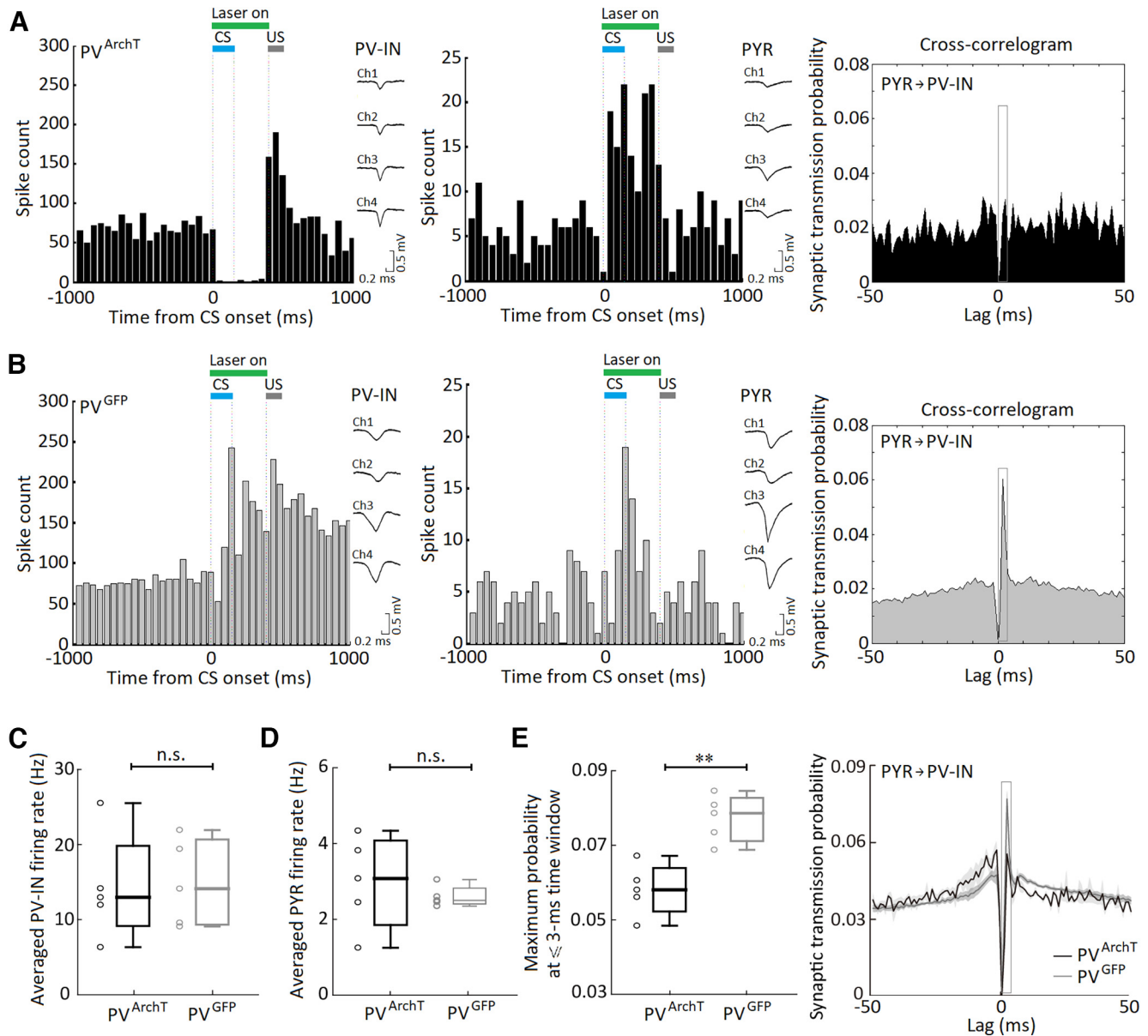


Figure 9. Optogenetic suppression of PV-IN sustained activity disrupts the hippocampal PYR-PVIN interaction at the early stage of tEBC acquisition. **A**, Left, Representative peristimulus time histogram (PSTH) shows optogenetic suppression of PV-IN sustained activity in a *PV^{ArchT}* mouse. The spike waveform of the PV-IN is illustrated. Middle, Representative PSTH shows the disinhibition of PYR activity when the PV-IN sustained activity was suppressed. The spike waveform of the PYR was also illustrated. Calibration: 0.5 mV for spike amplitude and 0.2 ms for time. Right, The CCG between the PYR and PV-IN spiking for the *PV^{ArchT}* mouse during tEBC training. **B**, Left, Representative PSTH shows the effect of green laser stimulation on PV-IN sustained activity in a *PV^{GFP}* mouse. The spike waveform of the PV-IN is illustrated. Middle, Representative PSTH shows PYR activity when green laser stimulation was delivered. The spike waveform of the PYR is also shown. Calibration: 0.5 mV for spike amplitude and 0.2 ms for time. Right, The CCG between the PYR and PV-IN spiking in the *PV^{GFP}* mouse during tEBC training. **C**, Average firing rates of hippocampal PV-INs during tEBC training for the *PV^{ArchT}* ($n = 5$, black) and *PV^{GFP}* ($n = 5$, gray) mice. **D**, Average firing rates of hippocampal PYRs during tEBC training for the *PV^{ArchT}* ($n = 5$, black) and *PV^{GFP}* ($n = 5$, gray) mice. **E**, Left, The spike transmission probability between PYR-PVIN pairs in *PV^{ArchT}* ($n = 5$, black) mice was lower than in *PV^{GFP}* ($n = 5$, gray) mice. Right, Averaged CCG between PYRs and PV-INs recorded from the *PV^{ArchT}* ($n = 5$, black) and *PV^{GFP}* ($n = 5$, gray) mice. Shading represents SEM. Calibration: **A**, **B**, Spike amplitude 0.5 mV or 0.2 ms for time. **C–E**, Box plots show median \pm IQR, whiskers show range. ** $p < 0.01$, n.s. $p > 0.05$.

To confirm the involvement of PV-IN sustained activity in hippocampal oscillatory activity was limited to occur in the CS-US interval period, we also observed the change of oscillatory activities during the US period. It was found that suppression of the PV-IN sustained activity seemed not to influence either gamma (35–85 Hz, $4.3 \pm 1.2\%$, $n = 7$ for *PV^{ArchT}* mice vs $1.9 \pm 0.8\%$, $n = 7$ for *PV^{GFP}* mice, $t_{(12)} = 1.800$, $p = 0.097$, independent t test; Fig. 10C) or theta band oscillation (5–12 Hz, $19.6 \pm 8.2\%$, $n = 7$ for *PV^{ArchT}* mice vs $6.2 \pm 4.3\%$, $n = 7$ for *PV^{GFP}* mice, $t_{(12)} = 1.556$, $p = 0.146$, independent t test; Fig. 10C) in the US period.

Gamma frequency entrainment early in learning accelerates subsequent tEBC acquisition

Suppression of the PV-IN sustained activity impaired both the augmentation of gamma band oscillation in CS-US interval and the acquisition of tEBC. These findings raise a possibility that the augmentation of gamma band oscillation in CS-US interval may be beneficial for the acquisition of tEBC. Therefore, we optogenetically activated the hippocampal PV-INs during the CS-US interval period at gamma frequency (40 Hz) early in learning to see whether the mice could show an increased learning rate compared with controls. To do this, we selectively expressed

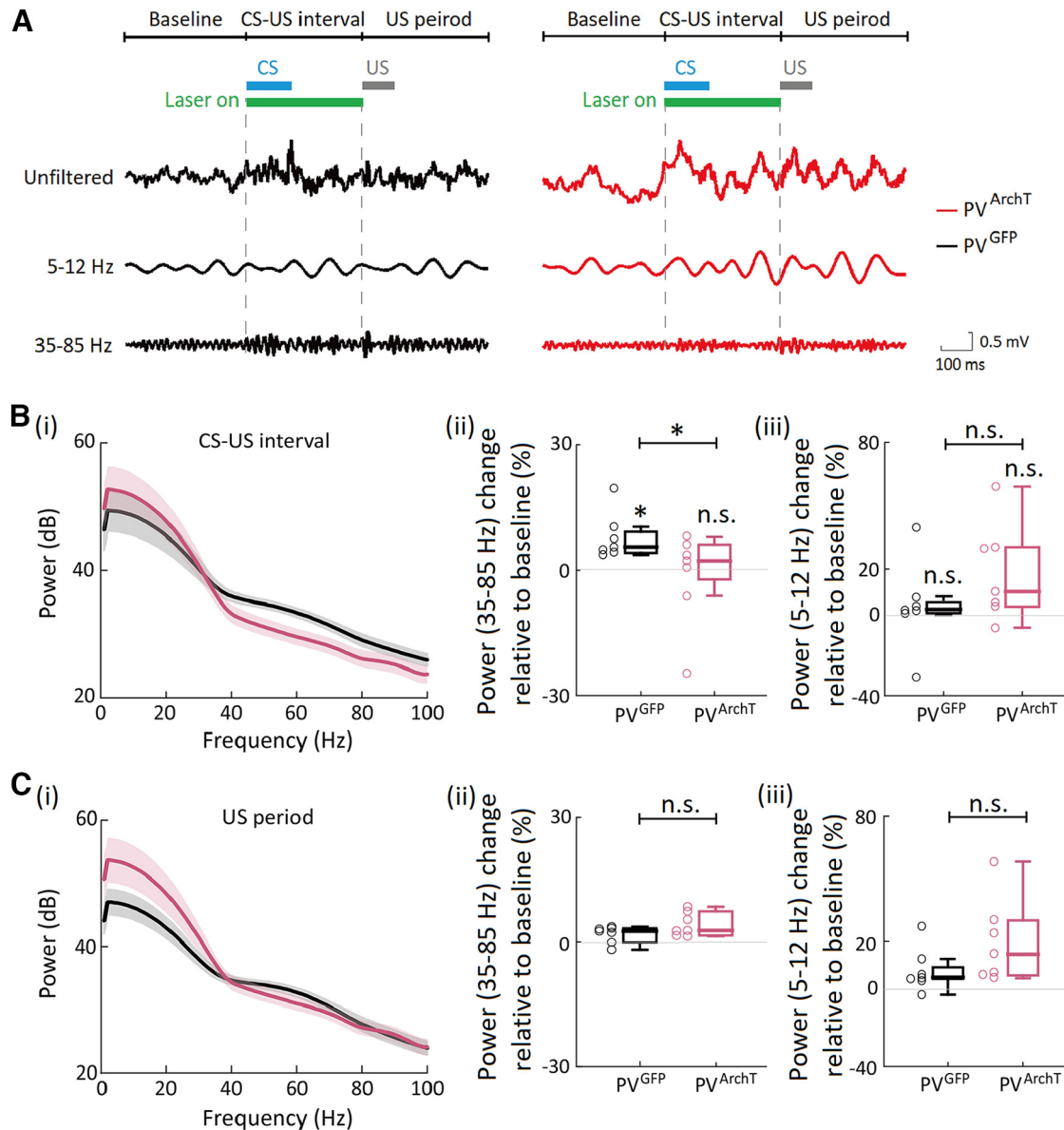


Figure 10. Attenuated gamma band oscillation by optogenetic suppression of PV-IN sustained activity. **A**, Left, Example traces showing the effect of green laser stimulation on LFP oscillation in the hippocampus of a PV^{GFP} mouse. The theta (5–12 Hz) and gamma band (35–85 Hz) filtered activities from a representative LFP are shown in black traces. Note increased amplitude in gamma band oscillation after the CS onset. Right, Example traces showing the effect of PV-IN sustained activity suppression on LFP oscillation in the hippocampus of a PV^{ArchT} mouse. The theta (5–12 Hz) and gamma band (35–85 Hz) filtered activities from a representative LFP were shown in red traces. CS, blue bar; US, gray bar. Calibration: 0.5 mV for LFP amplitude or 100 ms for time. **B**–**iii**, Average LFP power spectra (i) from the PV^{ArchT} ($n = 7$, pink) and PV^{GFP} ($n = 7$, black) mice during the CS-US interval period. The change of gamma band (35–85 Hz) oscillation during the CS-US interval period in PV^{ArchT} mice ($n = 7$, pink, ii) and PV^{GFP} ($n = 7$, black) mice (iii). The change of theta band (5–12 Hz) oscillation during the CS-US interval period in PV^{ArchT} mice ($n = 7$, pink) and PV^{GFP} ($n = 7$, black) mice (iii). **C**–**iii**, Average LFP power spectra from the PV^{ArchT} ($n = 7$, pink, i) and PV^{GFP} ($n = 7$, black) mice during the US period. The change of gamma band (35–85 Hz) oscillation during the US period in PV^{ArchT} mice ($n = 7$, pink) and PV^{GFP} ($n = 7$, black) mice (ii). The change of theta band (5–12 Hz) oscillation during the US period in PV^{ArchT} mice ($n = 7$, pink) and PV^{GFP} ($n = 7$, black) mice (iii). **Bi**, **Ci**, Shading represents SEM. **Bii**, **Biii**, **Cii**, **Ciii**, Box plots show median \pm IQR, whiskers show range. * $p < 0.01$, n.s. $p > 0.05$.

excitatory opsin ChR2 in bilateral dorsal hippocampus of PV-Cre mice (Fig. 11A,B). As illustrated in Figure 11C, 40 Hz (triggered by the CS onset, 10 ms laser on and 15 ms laser off, 400 ms in duration) blue laser stimulation of the hippocampal PV-INs evoked augmented gamma frequency oscillation during the CS-US interval period in a PV^{ChR2} mouse instead of in a $PV^{mCherry}$ mouse. Intriguingly, augmented gamma frequency (40 Hz) oscillation during the CS-US interval period at the ELS (days 1–2) was predictive of an increased learning rate on subsequent training days (days 3–5, training days effect, CR incidence, $F_{(1,10)} = 39.003$, $p < 0.001$; CR peak amplitude, $F_{(1,10)} = 0.420$, $p = 0.532$; training days times groups interaction, CR

incidence, $F_{(2,20)} = 0.064$, $p = 0.938$; CR peak amplitude, $F_{(2,20)} = 1.164$, $p = 0.332$; two-way ANOVA with repeated measures; Fig. 11D,E). Together, our results suggest that the PV-IN sustained activity is involved in the augmentation of gamma oscillation during the CS-US interval period, which is beneficial for the acquisition of tEBC.

Discussion

Using a combination of multichannel recording and optogenetics, we revealed that the hippocampal PV-INs showed CS-evoked firing activity during tEBC acquisition. In particular, the

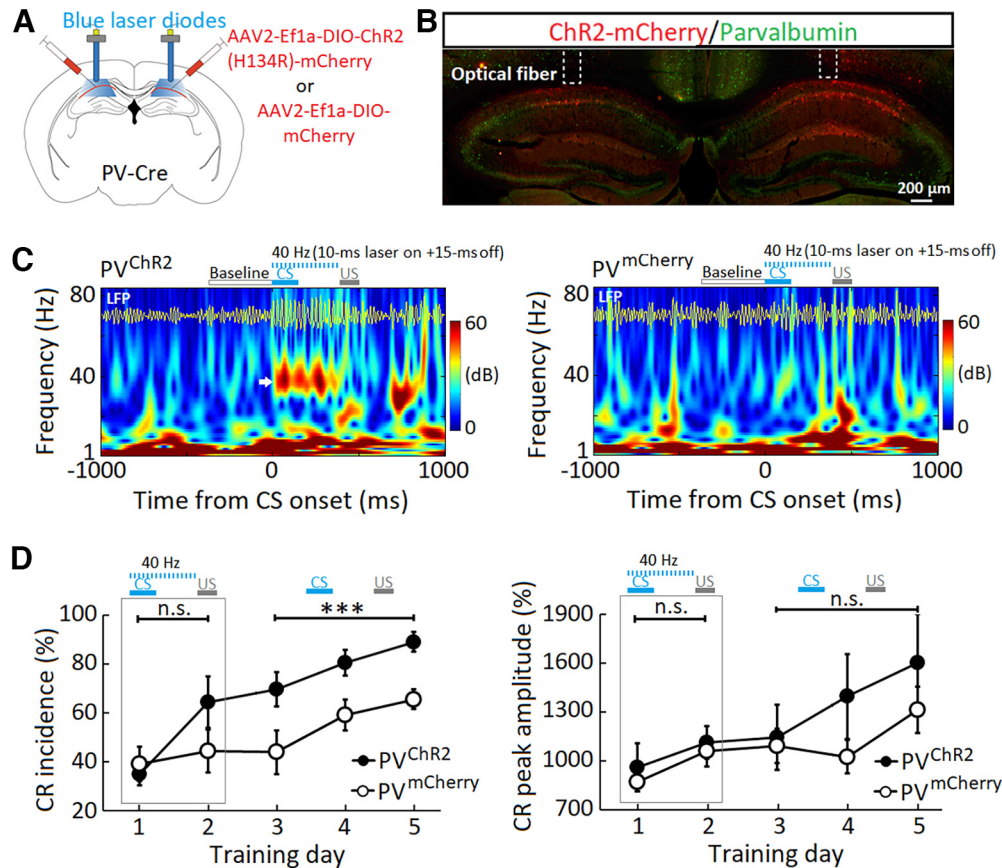


Figure 11. Gamma frequency entrainment accelerates the acquisition of tEBC. **A**, Schematic drawing shows optogenetic stimulation in bilateral dorsal hippocampus of PV-Cre mice. **B**, Coronal section of a PV-Cre mouse brain showing ChR2-mCherry expression (red) stained with parvalbumin (green) in bilateral dorsal hippocampus. Scale bar, 200 μ m. **C**, Left, Representative spectrogram showing gamma frequency oscillations (indicated by white arrow) evoked by 40 Hz blue laser stimulations (10 ms laser on and 15 ms laser off, 400 ms in duration) on the hippocampal PV-INs in a PV^{ChR2} mouse. The 40 Hz blue laser stimulations were triggered by the onsets of CSs. Right, Spectrogram showing that no obvious gamma frequency oscillations evoked by 40 Hz blue laser stimulations in a PV^{mCherry} mouse. CS, blue bar; US, gray bar. LFP, 35–85 Hz bandpass filtered. **D**, CR incidence and CR magnitude measured across five training days in PV^{ChR2} (filled circles, $n = 6$) and PV^{mCherry} (open circles, $n = 6$) mice. The presentations of CSs triggered 40 Hz blue laser stimulations on training days 1 and 2. Each blue laser stimulation lasted 400 ms. Data are presented as mean \pm SEM. *** $p < 0.001$, n.s. $p > 0.05$.

PV-IN firing activity was sustained from the CS presentation to the trace interval and was correlated with the CR occurrence. Selective suppression of the PV-IN sustained activity disrupted the PYR-PVIN interaction and attenuated gamma band oscillation during tEBC acquisition. Selective suppression of the PV-IN sustained activity caused impairment in tEBC acquisition. These results indicate that the hippocampal interneuron is a crucial cellular component of the associative learning network, and sustained activity of its PV-IN subtype plays a key role in associative learning.

There is growing evidence indicating an involvement of hippocampal interneurons in associative learning (Fuchs et al., 2007; He et al., 2021; Zhang et al., 2021). However, the mechanisms by which the hippocampal interneurons participate in associative learning remain not fully understood. In particular, considering the diversity of hippocampal interneurons (Freund and Buzsáki, 1996; Parra et al., 1998; Pelkey et al., 2017), a question remains about the contribution of a specific subtype of hippocampal interneurons to associative learning. We herein observed a learning-associated sustained activity in the hippocampal PV-INs during tEBC acquisition (Fig. 3). Importantly, the PV-IN sustained activity was biased between the CR and no-CR trials with greater firing responses in CR state (Fig. 4). We thus expected that the PV-IN sustained activity might contribute to the acquisition of tEBC. In support of this expectation, we

revealed that selective suppression of the PV-IN sustained activity impaired the tEBC acquisition (Fig. 5). Our findings not only add new data that the hippocampal PV-INs are critically involved in tEBC acquisition but also suggest that the sustained activity of hippocampal PV-INs is a candidate cellular mechanism supporting associative learning.

Accumulating evidence suggests that the acquisition of tEBC relies on a distributed forebrain network (Woodruff-Pak and Disterhoft, 2008; Weiss and Disterhoft, 2011) and that areas in this forebrain network communicate with each other (Takehara-Nishiuchi et al., 2012; Shearkhani and Takehara-Nishiuchi, 2013). Among the forebrain areas, the hippocampus is considered a hub because lesion or inactivation of the dorsal hippocampus results in severe impairment in the acquisition of tEBC (Solomon et al., 1986; Moyer et al., 1990; Weiss et al., 1999; Tseng et al., 2004; Sakamoto et al., 2005). Intriguingly, the hippocampus connects with several forebrain areas such as the prefrontal cortex (Jay and Witter, 1991; Cenquizca and Swanson, 2007) and the entorhinal cortex (Amaral and Witter, 1989; Rozov et al., 2020), which have been demonstrated to be critically involved in tEBC (Weible et al., 2000; Ryou et al., 2001; Siegel et al., 2015; Tanninen et al., 2015; Chen et al., 2016). Electrophysiological studies have documented that a number of hippocampal PYRs exhibited sustained excitatory activity in the CS-US interval during tEBC, whereas a larger

number of hippocampal PYRs showed sustained inhibitory activity (McEchron and Disterhoft, 1997; Hattori et al., 2015; Zhang et al., 2021; Li et al., 2022). Likewise, both sparse excitatory and strong inhibitory activities were observed in the hippocampal PYRs during appetitive auditory trace conditioning (Klee et al., 2021). The excitation mixed with stronger inhibition has been hypothesized to increase the signal-to-noise ratio of hippocampal PYR encoding for the CS-US association (Hattori et al., 2015). Here, we showed evidence that the PV-INs received augmented inputs from the excitatory PYRs during tEBC acquisition (Fig. 8). Anatomically, the hippocampal PV-INs in turn innervate the soma and proximal dendrites of local PYRs (Hu et al., 2014; Amilhon et al., 2015). Consequently, it is reasonable to propose that the PV-INs may efficiently cooperate with the PYRs to augment the signal-to-noise ratio of hippocampal encoding and thereafter contribute to inter-brain-area communication.

Our results revealed that the requirement of hippocampal PV-IN sustained activity for tEBC underwent dynamic change across associative learning. This view was supported by several facets of evidence in this study. First, the PV-IN sustained activity diminished at the LLS (Fig. 3). Second, there was no significant difference in the PV-IN sustained activity between the CR and no-CR states at the LLS (Fig. 4). Third, suppression of the PV-IN sustained activity had no obvious effect on the performance of well learned CRs at the LLS (Fig. 5). Indeed, a number of studies have demonstrated that the hippocampus plays a time-limited role in the acquisition of tEBC, with greater contribution at the initial learning stage (Takehara et al., 2002, 2003). Therefore, our current findings indicate that the dynamic change of hippocampal PV-IN sustained activity may be a candidate cellular process reflecting the distinct involvement of hippocampus in tEBC acquisition at various learning stages.

Although the role of hippocampal PV-IN sustained activity has been revealed in the acquisition of tEBC, how it forms is still a mystery. Previous studies have suggested that the entorhinal cortex can support the development of hippocampal neuronal activity that bridges time-separated stimuli (Suh et al., 2011; Kitamura et al., 2015; Qin et al., 2018). Consequently, the entorhinal cortical input to the hippocampus might be one of the sources contributing to the formation of PV-IN sustained activity. However, it should be noted that the PV-INs also receive excitatory inputs from neighboring PYRs within the hippocampus (Gulyás et al., 1993; English et al., 2017). Here, we found a learning-associated augmentation in the excitatory PYR-to-PVIN drive, which was positively correlated with the CR occurrence (Fig. 8). Because the hippocampal PYRs elevated their firing during the CS-US interval period, it is reasonable for us to propose that the augmented excitatory PYR-to-PVIN drive can contribute to the PV-IN sustained activity either. Indeed, modified hippocampal excitatory PYR-to-interneuron drive strength has been observed after spatial learning (Dupret et al., 2013; Gridchyn et al., 2020). Given this evidence, it seems possible that learning-associated modification of the hippocampal pyramidal-interneuron connection is the other mechanism to shape the PV-IN firing kinetics, which remodels the hippocampal network (Udakis et al., 2020; He et al., 2021).

Our results revealed that selective suppression of the PV-IN sustained activity reduced learning-associated augmentation of gamma band (35–85 Hz) oscillation during the CS-US interval period (Fig. 10), indicating a critical involvement of PV-IN sustained activity in influencing hippocampal oscillatory state

during tEBC acquisition. Previous studies have demonstrated that conditional ablation of the GluR-A subunit or γ CamKII in PV-INs could disrupt the PYR-to-PV-IN interaction and reduce the power of hippocampal gamma oscillation (Fuchs et al., 2007; He et al., 2021). Therefore, our observation of reduced gamma oscillation during the CS-US interval period was most likely because of the disrupted PYR-to-PV-IN interaction after suppression of the PV-IN sustained activity. Nevertheless, we did not observe significant changes in theta band (5–12 Hz) oscillation after the PV-IN suppression. This result was unexpected because theta band oscillation has been suggested to be highly correlated with tEBC (Wikgren et al., 2010; Darling et al., 2011). One explanation for this result is that other subtypes of hippocampal interneurons, in addition to the PV-INs, are also involved in theta band oscillation during tEBC. This possibility is raised as tEBC training induces an increase in intrinsic excitability of somatostatin-positive hippocampal interneurons (McKay et al., 2013). Consequently, intact theta band oscillation might result from our selective interrogation on the PV-INs. At the circuit level, theta-gamma coupling has been suggested to be an important mechanism subserving the communication among distributed brain areas during associative learning (Igarashi et al., 2014; Tanninen et al., 2017). Considering the evidence, we speculated that the diminished gamma but intact theta band oscillation might reduce theta-gamma coupling strength, and thus impaired the communication between the hippocampus and extrahippocampal structures during tEBC.

It should be noted that inhibition of PV-INs might disinhibit local PYRs (Fig. 9A, middle), which in turn caused an increased drive from the PYRs to PV-INs. Nevertheless, the PV-INs did not respond to the increased drive because they were inhibited by opsin ArchT (Fig. 9A, left). Our method did not aim to reduce excitatory drive from the PYRs to PV-INs. Instead, it aimed to disrupt the interaction between the PYRs and PV-INs during tEBC acquisition. Therefore, future experiments should be guaranteed to specifically interrogate excitatory drive from the hippocampal PYRs to PV-INs during tEBC.

Similar to the findings reported by Hattori et al. (2015), we observed that the hippocampal PYRs continued to respond to the CS at the LLS (Fig. 7). Although strong PYR inputs existed, however, the PV-INs did not maintain the sustained activity at this stage (Fig. 8). One explanation for this result is that synaptic transmission between hippocampal PYRs and PV-INs might endure plastic change across learning (Dupret et al., 2013; He et al., 2021). Alternatively, the PV-INs receive inputs from both extrahippocampal neurons (i.e., entorhinal cortex) and neighboring PYRs at the ELS, whereas they only receive inputs from neighboring PYRs at the LLS (Takehara-Nishiuchi et al., 2012).

In summary, our results outline a casual role for hippocampal PV-INs in associative learning. Moreover, we provide a mechanistic understanding of the kinetics of PV-IN activity that influences hippocampal network oscillatory state to support associative learning. Together, our data suggest that the recruitment of PV-INs into heterogeneous hippocampal network oscillatory patterns subserve the key aspect of associative learning.

References

- Amaral DG, Witter MP (1989) The three-dimensional organization of the hippocampal formation: a review of anatomical data. *Neuroscience* 31:571–591.
- Amilhon B, Huh CYL, Manseau F, Ducharme G, Nichol H, Adamantidis A, Williams S (2015) Parvalbumin interneurons of hippocampus tune population activity at theta frequency. *Neuron* 86:1277–1289.

- Antonoudiou P, Tan YL, Kontou G, Upton AL, Mann EO (2020) Parvalbumin and somatostatin interneurons contribute to the generation of hippocampal gamma oscillations. *J Neurosci* 40:7668–7687.
- Barthó P, Hirase H, Monconduit L, Zugaro M, Harris KD, Buzsáki G (2004) Characterization of neocortical principal cells and interneurons by network interactions and extracellular features. *J Neurophysiol* 92:600–608.
- Cenquizca LA, Swanson LW (2007) Spatial organization of direct hippocampal field CA1 axonal projections to the rest of the cerebral cortex. *Brain Res Rev* 56:1–26.
- Chen H, Wang YJ, Yang L, Sui JF, Hu ZA, Hu B (2016) Theta synchronization between medial prefrontal cortex and cerebellum is associated with adaptive performance of associative learning behavior. *Sci Rep* 6:20960.
- Chen JF, Liu K, Hu B, Li RR, Xin W, Chen H, Wang F, Chen L, Li R-X, Ren S-Y, Xiao L, Chan JR, Mei F, (2021) Enhancing myelin renewal reverses cognitive dysfunction in a murine model of Alzheimer's disease. *Neuron* 109:2292–2307.e5.
- Csicsvari J, Hirase H, Czurko A, Buzsáki G (1998) Reliability and state dependence of pyramidal cell-interneuron synapses in the hippocampus. *Neuron* 21:179–189.
- Csicsvari J, Hirase H, Czurkó A, Mamiya A, Buzsáki G (1999) Oscillatory coupling of hippocampal pyramidal cells and interneurons in the behaving rat. *J Neurosci* 19:274–287.
- Darling RD, Takatsuki K, Griffin AL, Berry SD (2011) Eyeblink conditioning contingent on hippocampal theta enhances hippocampal and medial prefrontal responses. *J Neurophysiol* 105:2213–2224.
- Dupret D, O'Neill J, Csicsvari J (2013) Dynamic reconfiguration of hippocampal interneuron circuits during spatial learning. *Neuron* 78:166–180.
- English DF, McKenzie S, Evans T, Kim K, Yoon E, Buzsáki G (2017) Pyramidal cell-interneuron circuit architecture and dynamics in hippocampal networks. *Neuron* 96:505–520.e7.
- Franklin KB, Paxinos G (2008) The mouse brain in stereotaxic coordinates. New York: Academic.
- Freund TF, Buzsáki G (1996) Interneurons of the hippocampus. *Hippocampus* 6:347–470.
- Fuchs EC, Zivkovic AR, Cunningham MO, Middleton S, Lebeau FEN, Bannerman DM, Rozov A, Whittington MA, Traub RD, Rawlins JNP, Monyer H (2007) Recruitment of parvalbumin-positive interneurons determines hippocampal function and associated behavior. *Neuron* 53:591–604.
- Galarreta M, Hestrin S (2001) Spike transmission and synchrony detection in networks of GABAergic interneurons. *Science* 292:2295–2299.
- Gridchyn I, Schoenenberger P, O'Neill J, Csicsvari J (2020) Optogenetic inhibition-mediated activity-dependent modification of CA1 pyramidal-interneuron connections during behavior. *Elife* 9:e61106.
- Gulyás AI, Miles R, Sik A, Tóth K, Tamamaki N, Freund TF (1993) Hippocampal pyramidal cells excite inhibitory neurons through a single release site. *Nature* 366:683–687.
- Harris KD, Henze DA, Csicsvari J, Hirase H, Buzsáki G (2000) Accuracy of tetrode spike separation as determined by simultaneous intracellular and extracellular measurements. *J Neurophysiol* 84:401–414.
- Hattori S, Chen L, Weiss C, Disterhoft JF (2015) Robust hippocampal responsiveness during retrieval of consolidated associative memory. *Hippocampus* 25:655–669.
- Hazan L, Zugaro M, Buzsáki G (2006) Klusters, NeuroScope, NDManager: a free software suite for neurophysiological data processing and visualization. *J Neurosci Methods* 155:207–216.
- He X, Li J, Zhou G, Yang J, McKenzie S, Li Y, Li W, Yu J, Wang Y, Qu J, Wu Z, Hu H, Duan S, Ma H (2021) Gating of hippocampal rhythms and memory by synaptic plasticity in inhibitory interneurons. *Neuron* 109:1013–1028.e9.
- Hu H, Gan J, Jonas P (2014) Interneurons. Fast-spiking, parvalbumin⁺ GABAergic interneurons: from cellular design to microcircuit function. *Science* 345:1255263.
- Igarashi KM, Lu L, Colgin LL, Moser MB, Moser EI (2014) Coordination of entorhinal-hippocampal ensemble activity during associative learning. *Nature* 510:143–147.
- Jay TM, Witter MP (1991) Distribution of hippocampal CA1 and subicular efferents in the prefrontal cortex of the rat studied by means of anterograde transport of Phaseolus vulgaris-leucoagglutinin. *J Comp Neurol* 313:574–586.
- Kitamura T (2017) Driving and regulating temporal association learning coordinated by entorhinal-hippocampal network. *Neurosci Res* 121:1–6.
- Kitamura T, Macdonald CJ, Tonegawa S (2015) Entorhinal-hippocampal neuronal circuits bridge temporally discontinuous events. *Learn Mem* 22:438–443.
- Klausberger T, Magill PJ, Márton LF, Roberts JDB, Cobden PM, Buzsáki G, Somogyi P (2003) Brain-state- and cell-type-specific firing of hippocampal interneurons *in vivo*. *Nature* 421:844–848.
- Klee JL, Souza BC, Battaglia FP (2021) Learning differentially shapes prefrontal and hippocampal activity during classical conditioning. *Elife* 10:e65456.
- Koh MT, Shao Y, Sherwood A, Smith DR (2016) Impaired hippocampal-dependent memory and reduced parvalbumin-positive interneurons in a ketamine mouse model of schizophrenia. *Schizophr Res* 171:187–194.
- Kotani S, Kawahara S, Kirino Y (2002) Classical eyeblink conditioning in decerebrate guinea pigs. *Eur J Neurosci* 15:1267–1270.
- Lapray D, Laszotzci B, Lagler M, Viney TJ, Katona L, Valenti O, Hartwich K, Borhegyi Z, Somogyi P, Klausberger T (2012) Behavior-dependent specialization of identified hippocampal interneurons. *Nat Neurosci* 15:1265–1271.
- Li R-R, Yan J, Chen H, Zhang W-W, Hu Y-B, Zhang J, Hu Z-A, Xiong Y, Yao Z-X, Hu B (2022) Sleep deprivation impairs learning-induced increase in hippocampal sharp wave ripples and associated spike dynamics during recovery sleep. *Cereb Cortex* 32:824–838.
- McEchron MD, Disterhoft JF (1997) Sequence of single neuron changes in CA1 hippocampus of rabbits during acquisition of trace eyeblink conditioned responses. *J Neurophysiol* 78:1030–1044.
- McEchron MD, Weible AP, Disterhoft JF (2001) Aging and learning-specific changes in single-neuron activity in CA1 hippocampus during rabbit trace eyeblink conditioning. *J Neurophysiol* 86:1839–1857.
- McKay BM, Oh MM, Disterhoft JF (2013) Learning increases intrinsic excitability of hippocampal interneurons. *J Neurosci* 33:5499–5506.
- Modi MN, Dhawale AK, Bhalla US (2014) CA1 cell activity sequences emerge after reorganization of network correlation structure during associative learning. *Elife* 3:e01982.
- Mount RA, Sridhar S, Hansen KR, Mohammed AI, Abdulkarim ME, Kessel R, Nazer B, Gritton HJ, Han X (2021) Distinct neuronal populations contribute to trace conditioning and extinction learning in the hippocampal CA1. *Elife* 10:e74730.
- Moyer JR Jr, Deyo RA, Disterhoft JF (1990) Hippocampectomy disrupts trace eye-blink conditioning in rabbits. *Behav Neurosci* 104:243–252.
- Nokia MS, Wikgren J (2014) Effects of hippocampal state-contingent trial presentation on hippocampus-dependent nonspatial classical conditioning and extinction. *J Neurosci* 34:6003–6010.
- Parra P, Gulyás AI, Miles R (1998) How many subtypes of inhibitory cells in the hippocampus? *Neuron* 20:983–993.
- Pelkey KA, Chittajallu R, Craig MT, Tricoire L, Wester JC, McBain CJ (2017) Hippocampal GABAergic inhibitory interneurons. *Physiol Rev* 97:1619–1747.
- Pilkiw M, Takehara-Nishiuchi K (2018) Neural representations of time-linked memory. *Neurobiol Learn Mem* 153:57–70.
- Qin H, Fu L, Hu B, Liao X, Lu J, He W, Liang S, Zhang K, Li R, Yao J, Yan J, Chen H, Jia H, Zott B, Konnerth A, Chen X (2018) A visual-cue-dependent memory circuit for place navigation. *Neuron* 99:47–55.e4.
- Rozov A, Rannap M, Lorenz F, Nasretudin A, Draguhn A, Egorov AV (2020) Processing of hippocampal network activity in the receiver network of the medial entorhinal cortex layer V. *J Neurosci* 40:8413–8425.
- Ryou JW, Cho SY, Kim HT (2001) Lesions of the entorhinal cortex impair acquisition of hippocampal-dependent trace conditioning. *Neurobiol Learn Mem* 75:121–127.
- Sakamoto T, Takatsuki K, Kawahara S, Kirino Y, Niki H, Mishina M (2005) Role of hippocampal NMDA receptors in trace eyeblink conditioning. *Brain Res* 1039:130–136.
- Shearkhani O, Takehara-Nishiuchi K (2013) Coupling of prefrontal gamma amplitude and theta phase is strengthened in trace eyeblink conditioning. *Neurobiol Learn Mem* 100:117–126.
- Siegel JJ, Taylor W, Gray R, Kalmbach B, Zemelman BV, Desai NS, Johnston D, Chitwood RA (2015) Trace eyeblink conditioning in mice is dependent upon the dorsal medial prefrontal cortex, cerebellum, and amygdala: behavioral characterization and functional circuitry. *eNeuro* 2:ENEURO.0051-14.2015.
- Solomon PR, Vander Schaaf ER, Thompson RF, Weisz DJ (1986) Hippocampus and trace conditioning of the rabbit's classically conditioned nictitating membrane response. *Behav Neurosci* 100:729–744.

- Strüber M, Sauer JF, Bartos M (2022) Parvalbumin expressing interneurons control spike-phase coupling of hippocampal cells to theta oscillations. *Sci Rep* 12:1362.
- Suh J, Rivest AJ, Nakashiba T, Tominaga T, Tonegawa S (2011) Entorhinal cortex layer III input to the hippocampus is crucial for temporal association memory. *Science* 334:1415–1420.
- Takehara K, Kawahara S, Takatsuki K, Kirino Y (2002) Time-limited role of the hippocampus in the memory for trace eyeblink conditioning in mice. *Brain Res* 951:183–190.
- Takehara K, Kawahara S, Kirino Y (2003) Time-dependent reorganization of the brain components underlying memory retention in trace eyeblink conditioning. *J Neurosci* 23:9897–9905.
- Takehara-Nishiuchi K, Maal-Bared G, Morrissey MD (2012) Increased entorhinal-prefrontal theta synchronization parallels decreased entorhinal-hippocampal theta synchronization during learning and consolidation of associative memory. *Front Behav Neurosci* 5:90.
- Tanninen SE, Yu X, Giritharan T, Tran L, Bakir R, Volle J, Morrissey MD, Takehara-Nishiuchi K (2015) Cholinergic, but not NMDA, receptors in the lateral entorhinal cortex mediate acquisition in trace eyeblink conditioning. *Hippocampus* 25:1456–1464.
- Tanninen SE, Nourizabari B, Morrissey MD, Bakir R, Dayton RD, Klein RL, Takehara-Nishiuchi K (2017) Entorhinal tau pathology disrupts hippocampal-prefrontal oscillatory coupling during associative learning. *Neurobiol Aging* 58:151–162.
- Tseng W, Guan R, Disterhoft JF, Weiss C (2004) Trace eyeblink conditioning is hippocampally dependent in mice. *Hippocampus* 14:58–65.
- Udakis M, Pedrosa V, Chamberlain SEL, Clopath C, Mellor JR (2020) Interneuron-specific plasticity at parvalbumin and somatostatin inhibitory synapses onto CA1 pyramidal neurons shapes hippocampal output. *Nat Commun* 11:4395.
- Wallenstein GV, Eichenbaum H, Hasselmo ME (1998) The hippocampus as an associator of discontinuous events. *Trends Neurosci* 21:317–323.
- Weible AP, McEchron MD, Disterhoft JF (2000) Cortical involvement in acquisition and extinction of trace eyeblink conditioning. *Behav Neurosci* 114:1058–1067.
- Weiss C, Disterhoft JF (2011) Exploring prefrontal cortical memory mechanisms with eyeblink conditioning. *Behav Neurosci* 125:318–326.
- Weiss C, Bouwmeester H, Power JM, Disterhoft JF (1999) Hippocampal lesions prevent trace eyeblink conditioning in the freely moving rat. *Behav Brain Res* 99:123–132.
- Wikgren J, Nokia MS, Penttonen M (2010) Hippocampo-cerebellar theta band phase synchrony in rabbits. *Neuroscience* 165:1538–1545.
- Witton J, Staniaszek LE, Bartsch U, Randall AD, Jones MW, Brown JT (2016) Disrupted hippocampal sharp-wave ripple-associated spike dynamics in a transgenic mouse model of dementia. *J Physiol* 594:4615–4630.
- Woodruff-Pak DS, Disterhoft JF (2008) Where is the trace in trace conditioning? *Trends Neurosci* 31:105–112.
- Zhang J, Zhang K-Y, Zhang L-B, Zhang W-W, Feng H, Yao Z-X, Hu B, Chen H (2019) A method for combining multiple-units readout of optogenetic control with natural stimulation-evoked eyeblink conditioning in freely-moving mice. *Sci Rep* 9:1857.
- Zhang J, Chen H, Zhang LB, Li RR, Wang B, Zhang QH (2022) Ventromedial thalamus-projecting DCN neurons modulate associative sensorimotor responses in mice. *Neurosci Bull* 38:459–473.
- Zhang LB, Zhang J, Sun MJ, Chen H, Yan J, Luo FL, Yao ZX, Wu YM, Hu B (2020) Neuronal activity in the cerebellum during the sleep-wakefulness transition in mice. *Neurosci Bull* 36:919–931.
- Zhang WW, Li RR, Zhang J, Yan J, Zhang QH, Hu ZA, Yao ZX, Chen H (2021) Hippocampal interneurons are required for trace eyeblink conditioning in mice. *Neurosci Bull* 37:1147–1159.